NAZARBAYEV UNIVERSITY

SCHOOL OF MINING AND GEOSCIENCES

Application of Machine Learning on Predicting Oil Recovery during Spontaneous Imbibition by Low Salinity Water

By

Azamat Bukayev

Supervisor: Dr. Masoud Riazi

Co-supervisor: Dr. Mian Umer Shafiq

Nazarbayev University

April 2025

ORIGINALITY STATEMENT

I, Azamat Bukayev, hereby declare that this submission is my own work and to the best of my knowledge it contains no materials previously published or written by another person, or substantial proportions of material which have been accepted for the award of any other degree or diploma at Nazarbayev University or any other educational institution, except where due acknowledgement is made in the thesis.

Any contribution made to the research by others, with whom I have worked at NU or elsewhere is explicitly acknowledged in the thesis.

I also declare that the intellectual content of this thesis is the product of my own work, except to the extent that assistance from others in the project's design and conception or in style, presentation, and linguistic expression is acknowledged.

Signed on 13.04.25

_____

ABSTRACT

This thesis explores how machine learning can be used to predict spontaneous imbibition recovery, the process where oil is naturally displaced by water in porous rock, such as in fractured reservoirs. Traditionally, running these lab experiments can take a lot of time, sometimes even months. Instead of waiting that long, this research gathers data from real laboratory results and applies different machine learning models to predict how much oil can be recovered. The focus is on using input parameters like core size, porosity, salinity, temperature, and more to estimate recovery performance without having to physically run the test every time. Six different models were tested: Artificial Neural Networks, Decision Tree, Gradient Boosting, Random Forest, Support Vector Machine, and Extreme Gradient Boosting. The performance of each model was evaluated based on how accurately it could predict real experimental outcomes. The Gradient Boosting model stood out as the most accurate, especially when trained on a combination of secondary and tertiary imbibition data. While the predictions were promising, the study also discusses the limitations of the current dataset and suggests that including more physical parameters like interfacial tension and contact angle could make future predictions even better. Overall, this work shows that machine learning has real potential to speed up and improve decision-making in enhanced oil recovery research.

ACKNOWLEDGMENT

I want to express my gratitude to my supervisor, Prof. Masoud Riazi, and my co-supervisor, Prof. Mian Umer Shafiq, for their guidance and support throughout my master's journey. Working under their guidance was a significant milestone in my academic career. It was a pleasure to work with such professional and kind people!

Also, I would like to thank my family and friends, who were always there with me. Special thanks to my loved one for always supporting me!

Table of Contents

List of Figures

List of Tables

Chapter 1: Introduction

First, oil is produced by the natural energy of the reservoir, known as primary production, which accounts for 5-20% of the total hydrocarbon reserves extracted. After that, an additional 15-35% of the total hydrocarbon production can be achieved by secondary recovery. Typically, water or gas injection is used to maintain the reservoir pressure at a sufficient level and to displace oil, thereby maintaining a certain level of production. When water or gas injection results in a decline in production, tertiary recovery is applied, such as in different EOR techniques.

Naturally fractured reservoirs comprise more than half of all oil reserves. An estimated 30% of global oil production comes from naturally fractured sources. Reservoirs with natural fractures are generally regarded as dual-porosity systems consisting of the fractures and the matrix, which are two different media. The fractures have very low porosity and significant permeability, whereas the matrix has low porosity. With the fracture system acting as the primary conduit for fluid transport, most of the oil is stored in the matrix. Therefore, it is a complex process to extract oil from this type of reservoir, especially at the later stages of the production when tertiary recovery methods need to be applied.

In such reservoirs, it is necessary to focus on EOR methods that increase oil production by imbibition, which is one of the governing processes of oil extraction from naturally fractured reservoirs. Imbibition is the process of displacing a wetting fluid by a nonwetting fluid via capillary action. In other words, the rock grains in the reservoir are enveloped by oil, and water displaces oil due to imbibition.

There are two types of imbibition: spontaneous imbibition and forced imbibition. Spontaneous imbibition is the process of displacing oil by water from rock grains under static conditions, where there is no injection or viscous force.

The demand for oil supply is rising all over the world, and it is necessary to produce oil from fractured oil-wet formations, which are complex in terms of oil extraction. One of the main reasons for the complexity of oil recovery in such formations is that common EOR techniques do not result in significant additional oil recovery. The problem with most traditional EOR techniques is that they work inefficiently in fractured oil-wet formations because imbibition is not being sufficiently affected, which is one of the governing processes of oil recovery in

such formations. Therefore, it is necessary to analyze different techniques to increase oil production in such fields.

Previously, researchers have investigated the effect of different EOR techniques on increasing oil recovery through imbibition. One method for increasing imbibition oil recovery is to use low-salinity water (LSW). LSW is a cheap alternative to other methods, which also increase the imbibition oil recovery, such as surfactants, alkali, or nanoparticles. LSW is becoming a common practice to be used in the industry.

Performing spontaneous imbibition experiments takes a lot of time and can last months to determine the effect of the imbibing fluid on oil recovery.

This work focuses on the application of machine learning models to predict spontaneous imbibition recovery experiments to determine the absolute oil recovery by different fluids. The results of the machine learning methods were compared to the real laboratory experiments, and a comprehensive analysis was performed to identify the most effective method.

Chapter 2: Literature Review

2.1. EOR methods

At the initial stage of field production, oil is produced at high reservoir pressure. This process is called primary oil extraction. Primary drive mechanisms such as water drive, gas-cap drive, solution-gas drive, and gravity drives maintain the reservoir pressure high (Smithson, 2016). Usually, during primary oil extraction, 5-20% of the total hydrocarbons from the reservoir can be recovered (Ragab and Mansour, 2021). At a certain point in time, oil extraction slows down because the natural energy of the reservoir is not enough, and the primary driving mechanisms start to weaken, to push hydrocarbons to the surface. When the production rate decreases and decreases beyond the optimum production range, a secondary stage of driving mechanisms is introduced. Secondary recovery occurs when gas or water is injected to sustain the reservoir pressure in the optimum range. Secondary oil extraction methods are used to increase oil production. Water or gas is injected into the reservoir through the injection wells to increase the reservoir pressure and maintain it at high levels. An additional 15–35% recovery is achieved after applying secondary oil recovery methods (Qisheng and Yongchun, 2023). However, due to the current increase in demand for oil in the global market, more oil needs to be supplied and produced. Therefore, tertiary oil recovery methods are applied if primary and secondary oil recovery methods are not sufficient to sustain sufficient oil production rates.

When secondary recovery methods start to lose their efficiency, further techniques such as tertiary oil recovery should be used (Nolan, 2010). Therefore, tertiary methods are mostly applied in mature oil fields (Maricic et al, 2014). Tertiary oil recovery or enhanced oil recovery (EOR) methods target immobile oil reserves that cannot be produced by primary or secondary recovery methods (Denney, 2012). EOR methods are applied to increase the production of oil from a reservoir and prolong the reservoir’s life and profitability. EOR methods are divided into four groups: thermal, gas injection, chemical, and microbial. Figure 1 shows the EOR technique classification (Muriel et al., 2020).

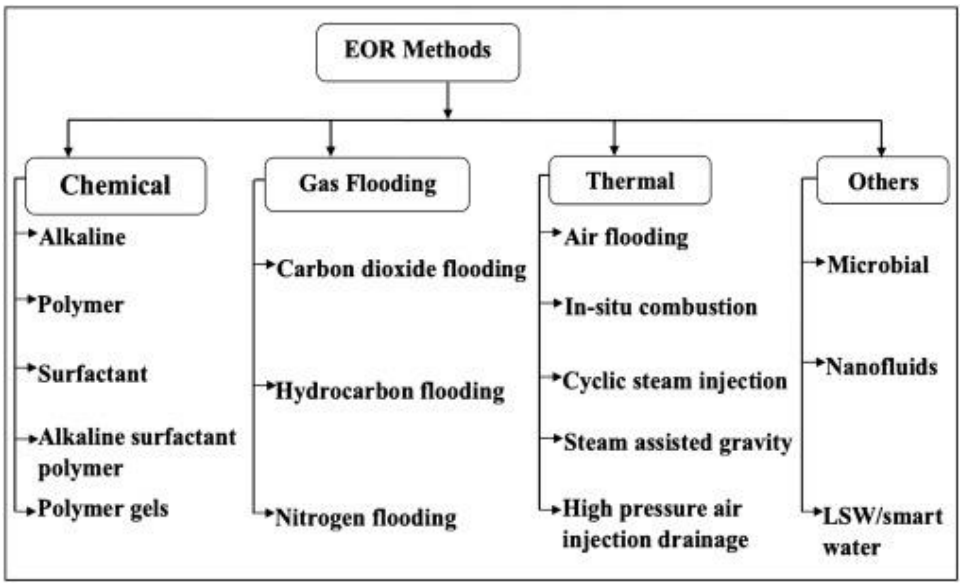

Figure 1. EOR method classification (Alfarge et al., 2020)

One way to increase spontaneous imbibition oil recovery is by applying LSW. It is becoming an increasingly popular method that is being applied in the industry because of its low cost and ease of application.

2.2. LSW mechanisms

Many researchers have studied the effects of salinity on oil–water infiltration and replacement. As for the change in rock surface wettability, Liu et al. (2022) stated that the main reason for the increase in oil recovery by low-salinity water flooding was that the low salinity could change the wettability of the rock surface, making the surface more hydrophilic. Mohammadi et al.'s (2019) experiment showed that low-salinity brine can reduce the wetting contact angle of carbonate rock from 114° to 42°, effectively enhancing imbibition and oil recovery. By measuring zeta potential, Tetteh et al. (2018) found that as salinity decreased, the charge on the rock surface also decreased, and the wettability of the rock changed from oil-wet to neutral-wet. Song et al. (2020) calculated the electrostatic component of the disjoining pressure to explain the change in wettability as a result of fewer Na+ surface complexes in low-salinity water. Hidayat et al.’s (2018) experiment showed that brine containing high Mg2+ and Ca2+ concentrations significantly improves the recovery efficiency of osmosis water. The reason for this situation, explained by Ghandi et al., was that brine containing divalent ions such as Mg2+ and Ca2+ could change the wettability of

lipophilic rock to low or neutral wettability, thus enhancing imbibition recovery (Ghandi et al., 2019).

Guo et al. (2020) investigated the effect of salinity on the mechanisms of imbibition. Spontaneous imbibition tests were conducted with a 7.39% porosity and 0.084 mD average air-permeability tight sandstone core to determine how different salinities affect imbibition recovery. Figure 2 shows the results of the tests. From that figure, it can be seen that the highest imbibition recovery was achieved by distilled water (23%), followed by water with 15000 ppm (10%), and water with 45000 ppm (5%). Additionally, the stability of imbibition recovery is achieved at different times depending on the salinity of the water. 48 hours for distilled water, 72 h for water with 15000 ppm salinity, and 144 h for water with 45000 ppm salinity. Therefore, salinity affects both imbibition recovery and the time necessary to achieve stable imbibition.

There are two main effects of salinity on the imbibition mechanism. First, the difference in salt concentration causes osmotic pressure, which transfers water molecules from low-salinity to high-salinity zones through a semipermeable membrane, caused by clay minerals. The second is that variation in salinity affects the IFT. At higher salinity, this effect is greater, and it takes more time for the imbibition process to stabilize.

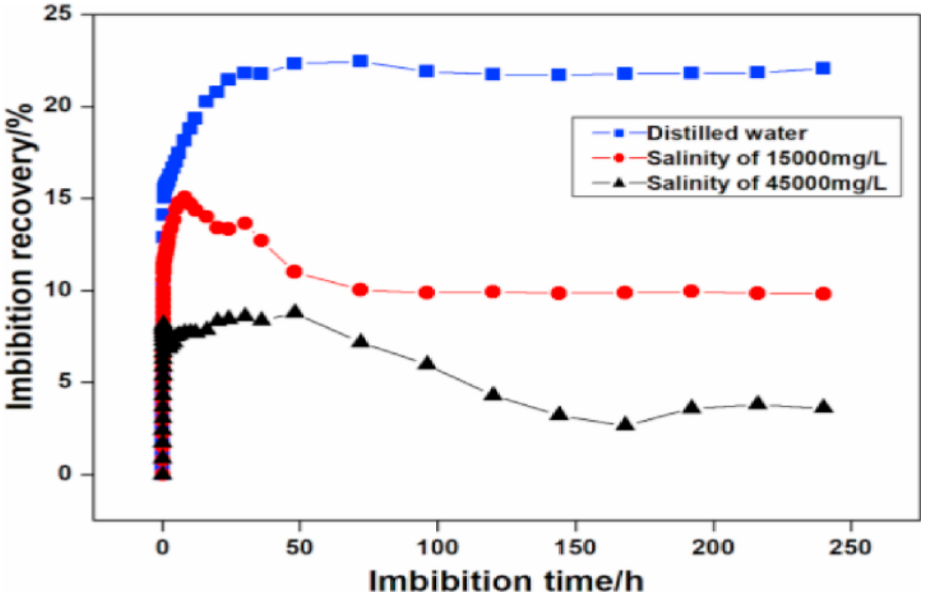

Figure 2. Relationship between imbibition recovery time and imbibition time under different salinity. (Gao et al., 2020)

Mahmoudzadeh et al. (2022) also investigated the effect of salinity on the imbibition process. This study focused on micromodels with different patterns as replications of spontaneous imbibition tests. The effect of low-salinity water on the spontaneous imbibition process is shown in Figure 3. From left to right, the size of the scale increases; patterns A-B are similar to spontaneous imbibition tests on a microscopic scale; patterns C-D are for fractured cores. The results show that with an increase in scale, low-salinity water (LSW) tends to decrease ultimate oil saturation.

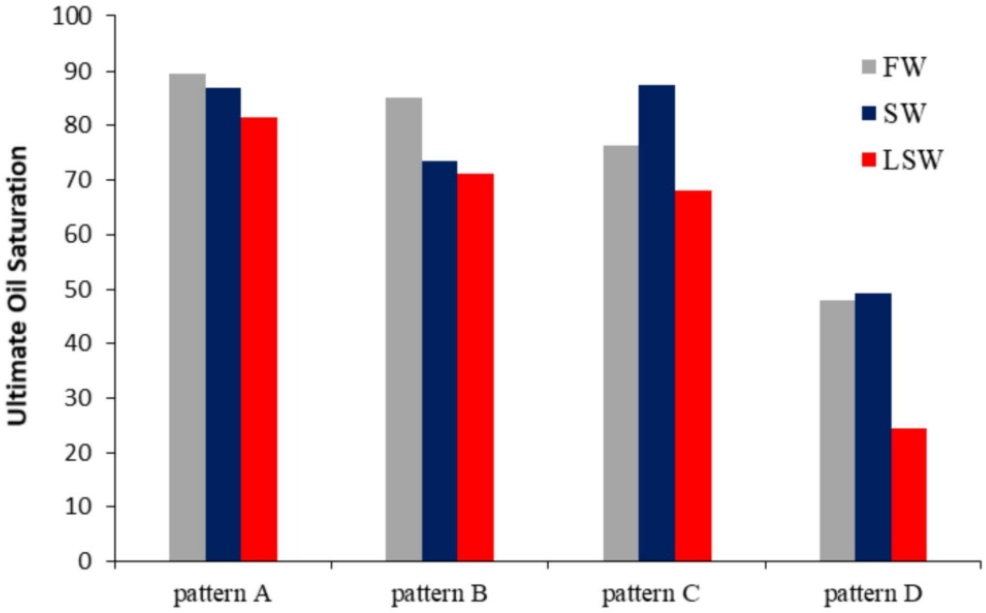

Figure 3. Ultimate oil recovery from different types of water (Mahmoudzadeh et al., 2022)

Zhang et al. (2018) investigated the effect of salinity on oil recovery in core flooding tests. Figure 4 shows the results of the core flooding tests. Zhang et al. stated that LSW resulted in 46.86% oil recovery, while high-salinity water (HSW) resulted in 36.19% oil recovery. An additional 10.67% of the oil recovery was achieved by the LSW. Both the spontaneous imbibition and core flooding tests show that low-salinity water has a positive effect on oil recovery.

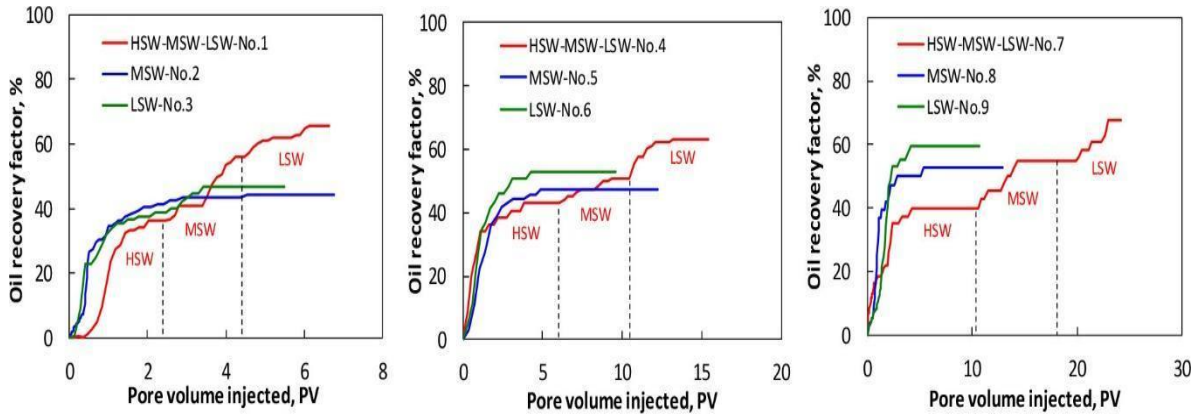

Figure 4. Core flooding tests were conducted using water with different salinities (Zhang et al., 2018)

2.3. Spontaneous Imbibition

Spontaneous imbibition (SI) refers to the natural absorption of a wetting fluid into a porous medium, which is predominantly driven by capillary forces (Morrow & Mason, 2001; Zhou et al., 2002). In petroleum reservoirs, this phenomenon plays a crucial role in enhancing oil recovery, particularly in fractured and heterogeneous reservoirs, where conventional recovery methods may not yield optimal results (Austad & Standnes, 2003; Tavassoli et al., 2005). Spontaneous imbibition relies heavily on the balance between capillary and viscous forces within the reservoir rock, influencing how effectively the water phase replaces oil within the pores (Behbahani et al., 2006).

The process of spontaneous imbibition is inherently linked to reservoir wettability, which is defined as the tendency of reservoir rock to preferentially attract and retain one fluid phase over another (Anderson, 1986; Buckley et al., 1998). Rocks can exhibit varying wettability states, including water-wet, oil-wet, or intermediate-wet conditions (Morrow, 1990; Zhang & Austad, 2006). The wettability state profoundly affects the imbibition dynamics, with strongly water-wet conditions generally favoring spontaneous imbibition processes and subsequent oil recovery (Standnes & Austad, 2000; Zhou et al., 2002). Conversely, oil-wet or neutral-wet conditions tend to hinder spontaneous imbibition, limiting oil displacement efficiency (Austad & Standnes, 2003; Morrow & Mason, 2001).

The significance of spontaneous imbibition is notably pronounced in fractured reservoirs, where a complex network of fractures and low-permeability matrix blocks exists (Behbahani et al., 2006; Tavassoli et al., 2005). Here, capillary forces are critical for transferring fluids between fractures, where injection fluids flow easily, and the tighter rock matrix, where substantial volumes of oil reside (Kazemi et al., 1976; Cil et al., 1998). The success of spontaneous imbibition in these scenarios can greatly determine overall reservoir performance and recovery efficiency, underscoring the importance of understanding and accurately modeling this phenomenon (Schechter et al., 1991; Behbahani et al., 2006).

Numerous experimental and theoretical studies have been conducted to understand spontaneous imbibition processes. The Amott test is an experimental technique commonly used to investigate spontaneous imbibition (Morrow, 1990; Mason & Morrow, 1994). As shown in Figure 5, the presence of fractures stimulates oil recovery via imbibition.

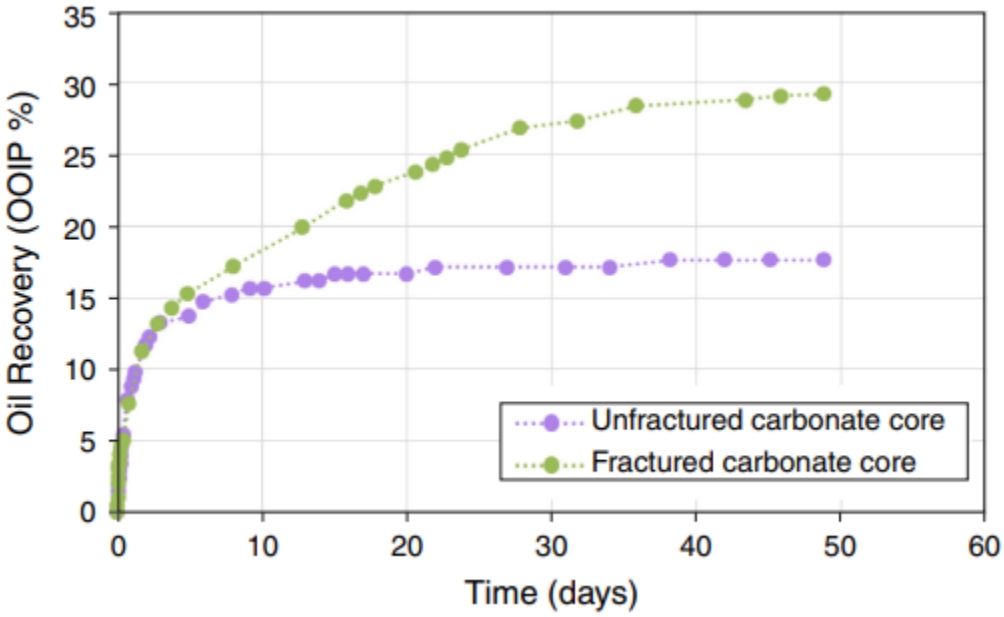

Figure 5. Influence of Fractures on Imbibition (Vilhena et al., 2020)

In naturally fractured reservoirs with low-permeability rock matrices, water capillary imbibition represents a critical process for oil recovery, causing oil to be displaced from the matrix blocks into neighboring fractures. This mechanism is particularly important in reservoirs where a highly permeable fracture network renders traditional production

techniques ineffective. A schematic representation of the imbibition process is presented in Figures 6 and 7.

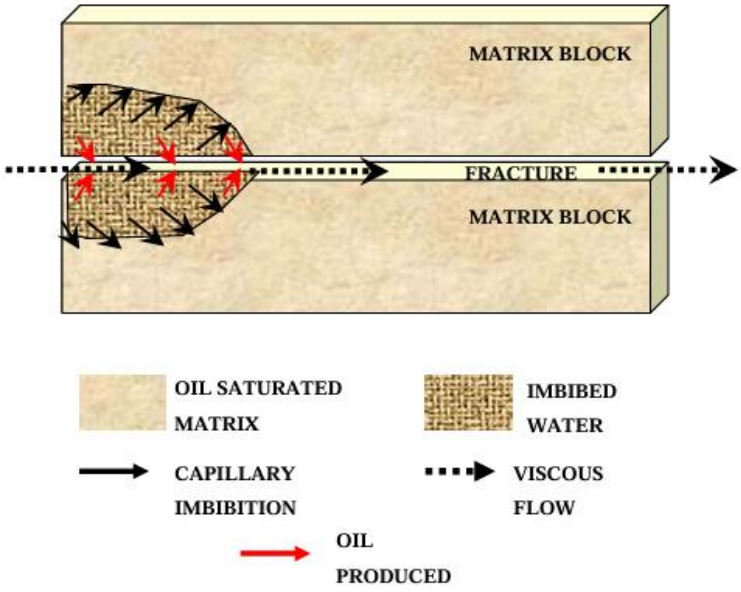

Figure 6. Scheme for Oil Production in Naturally Fractured Reservoirs (Patel & Meher, 2018)

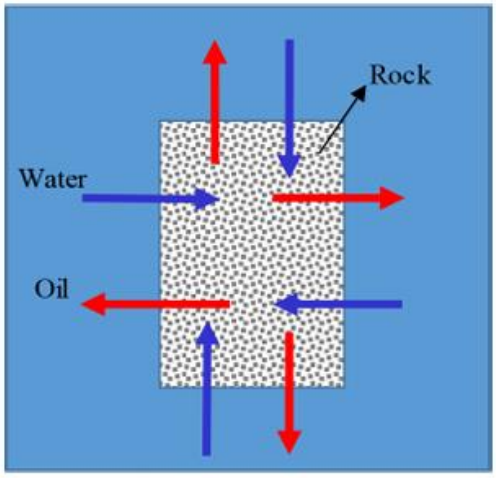

Figure 7. Schematic Representation of the Imbibition Process (Tian et al., 2021)

Alteration of the capillary can change the imbibition to fractures. There are two main ways in which EOR methods can change the capillary and increase oil recovery by imbibition: wettability alteration and IFT reduction. Producing oil from an oil-wet system is very challenging, which is why EOR methods, which can alter the wettability from oil-wet to water-wet, can significantly increase imbibition oil recovery. IFT reduction can significantly

increase imbibition oil recovery because high IFT does not allow water to mix with oil and recover it on the pore scale.

2.4. Secondary and Tertiary Spontaneous Imbibition Experiments

When studying spontaneous imbibition behavior in porous media—especially in the context of enhanced oil recovery—it's important to distinguish between secondary and tertiary spontaneous imbibition tests. These tests differ in terms of the sequence of fluid interactions they represent and are designed to simulate different stages of a reservoir's life cycle. Understanding both is essential because the oil recovery efficiency and the mechanisms at play can vary significantly depending on whether the porous medium is exposed to brine for the first time or has already undergone prior flooding (Zhou et al., 2002; Tavassoli et al., 2005).

Secondary spontaneous imbibition typically refers to the initial exposure of a porous rock sample, such as a sandstone or carbonate core, to a water-based fluid after saturation with oil. In a laboratory setting, this process is designed to mimic what happens when a water-based displacing fluid, like low-salinity brine or formation water, invades the reservoir for the first time after oil has displaced the original water (Ma et al., 1997).

In this test, the core sample is first cleaned, dried, and saturated with brine to achieve 100% water saturation. The reservoir is then flooded with crude oil (or a synthetic oil substitute) to the desired initial water saturation (Swi), which replicates the conditions of a reservoir after primary depletion. After aging to restore reservoir-like wettability conditions—especially important in oil-wet or mixed-wet systems—the sample is placed in contact with a brine bath, usually under ambient pressure and temperature, although some studies apply reservoir-like conditions (Standnes & Austad, 2000). Water spontaneously imbibes into the core, displacing oil due to capillary forces and possibly wettability alteration, depending on the fluid chemistry.

Secondary imbibition experiments are especially valuable for evaluating the base-case recovery potential of a reservoir under natural water drive or in the early stages of water injection. The total oil recovered and the recovery rate provide insights into the effectiveness of spontaneous imbibition as a mechanism in primary and secondary recovery operations.

These tests are commonly used to benchmark the impact of modifying the injected brine salinity, pH, or ionic composition (Morrow & Mason, 2001).

Tertiary spontaneous imbibition, on the other hand, occurs after a core has already undergone a prior flooding stage, typically with high-salinity brine. This setup is designed to replicate enhanced recovery conditions, where a new fluid (like low-salinity water, surfactant solution, or smart water) is introduced into a reservoir that has already been partially swept by conventional waterflooding (Austad et al., 2010).

In a laboratory setup, a typical tertiary test begins by preparing the core in the same way as in the secondary test. However, instead of directly subjecting the core to low-salinity brine, it first undergoes flooding or spontaneous imbibition with high-salinity water, which simulates the traditional secondary recovery stage. Once this initial imbibition reaches a plateau (i.e., little to no more oil is recovered), the test is paused. The fluid surrounding the core is then replaced with a tertiary fluid, such as a lower salinity brine, and imbibition is allowed to continue (Tang & Morrow, 1999).

The key purpose of tertiary imbibition tests is to observe whether additional oil recovery can be achieved after the high-salinity phase. These tests are especially crucial for validating the performance of low-salinity waterflooding (LSWF) strategies. If a significant volume of oil is recovered during the tertiary stage, this strongly supports the hypothesis that mechanisms like wettability alteration, double-layer expansion, and ion exchange are activated under low-salinity conditions. In other words, tertiary imbibition tests serve as proof-of-concept for many chemical EOR mechanisms (Zhang et al., 2007).

Another important finding from the tertiary tests is related to the sequence dependency of fluid interactions. In some cases, cores that exhibit limited recovery during secondary imbibition with formation water respond dramatically when exposed to low-salinity water in the tertiary phase, suggesting that prior exposure to high-salinity conditions can actually trigger or enhance the effect of LSWF later on (Sheng, 2014).

Studies of both secondary and tertiary imbibition give researchers and engineers a fuller picture of how a reservoir might behave throughout its lifecycle. Secondary tests provide a

baseline that shows what could happen under natural conditions or traditional waterflooding. By contrast, tertiary tests demonstrate the potential for unlocking residual oil after conventional methods have been exhausted.

For machine learning models and predictive frameworks, separating data into secondary and tertiary cases is also essential. Recovery factors, fluid interactions, and response patterns differ depending on the test type, and failing to account for these factors can lead to inaccurate predictions or misleading trends in model training.

2.5. Sources of Data

The data from 25 research papers were collected. The datasets consisted of information about laboratory spontaneous imbibition experiments using the Amott cell. The Amott cell shown in Figure 8 is one of the most frequently used instruments for conducting spontaneous imbibition tests. The main principle is that a saturated oil-filled core is placed into the cell. Then, the cell with the core is filled with brine solution, and oil is produced. The oil produced can be easily recorded according to the scale on the top part of the Amott cell.

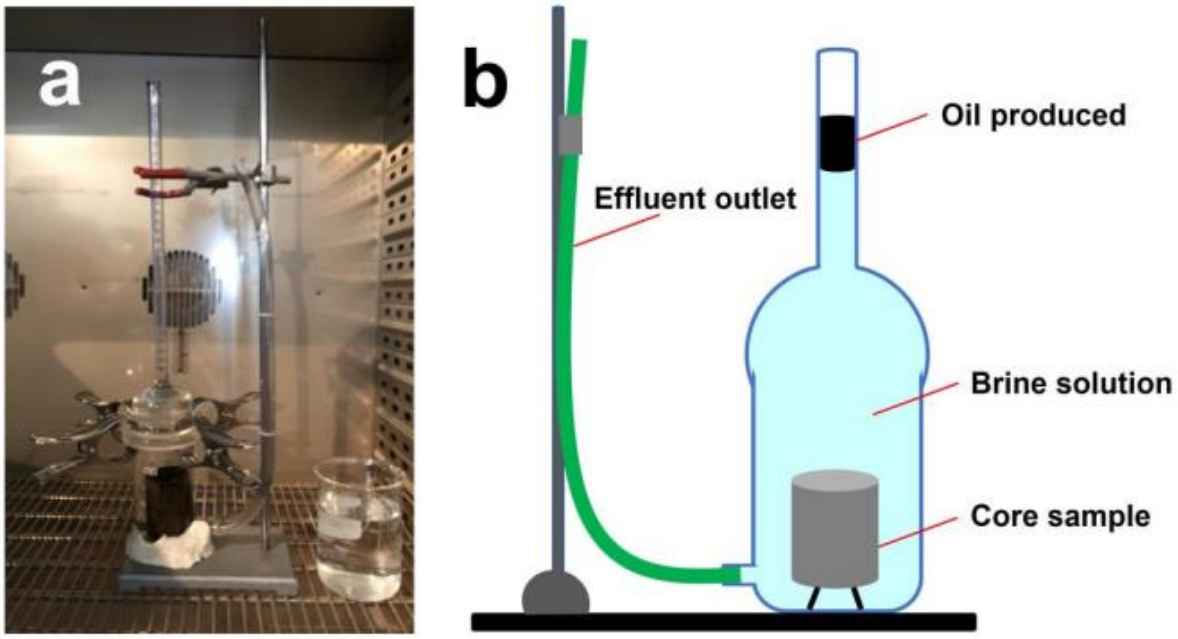

Figure 8. (a) Amott cell apparatus and (b) schematic representation of the Amott cell (Sukee et al., 2022)

The Amott cell can be used for both secondary and tertiary spontaneous imbibition experiments. The dataset for this study contains information on secondary spontaneous experiments, where the salinity of the brine remained constant, and tertiary spontaneous experiments, which utilized brines with varying salinity levels.

The input data were extracted from the studies. Core characteristics such as length, diameter, porosity, initial water saturation, and temperature of the experiment were usually extracted from the tables. An example of such a table is given in Table 1. The lithologies of the cores were classified as chalk being 1, sandstone being 2, and carbonate being 3. It is necessary to provide only numerical data to the machine learning models.

Table 1. Core characteristics (Fathi et al., 2010)

core ID	*L* (mm)	*D* (mm)	PV (mL)	Φ (%)	S_{wi} (%)	S_{oi} (%)	remarks
LSSK#5	70	38.1	37	46	10	90	initial wettability test
SCC#1	70	38.1	36	45	0	0	reference core
SCC#2	70	38	36	45	0	0	reference core
SK#8	69.9	38.1	37	47	9	91	SI at 100 °C
LSSK#7	70	38.1	36	45	9	91	SI at 100 °C
SK#12	69.8	37.8	35	45	9	91	SI at 100 °C
SF#14	70	38.1	36	45	8	92	SI at 110 °C and wettability test
SF#15	70	38.1	37	46	9	91	SI at 110 °C and wettability test
SF#18	70	38.1	36	46	8	92	SI at 110 °C
SF#9	70	38.1	37	46	9	91	SI at 110 °C and wettability test
LSSK#3	70	38.1	36	45	9	91	SI at 120 °C
SK#13	69.2	38.1	36	45	8	92	SI at 120 °C
LSSK#1	70	38.1	37	46	8	92	SI at 120 °C
LSSK#2	70	38.1	37	46	8	92	SI at 120 °C
LSSK#4	70	38.1	37	46	8	92	SI at 120 °C
SF#20	70	38.1	36	45	8	92	forced displacement
SF#16	70	38.1	36	45	10	90	forced displacement
SF#17	70	38.1	36	46	8	92	forced displacement

The Plot Digitizer tool was used to extract the absolute oil recovery values from the graphs of the recovery factor over time. An example of a graph from which the outputs were collected is shown in Figure 9. There were no tabular data on recovery factors available for most of the studies, so it was decided to extract data points manually from the graphs.

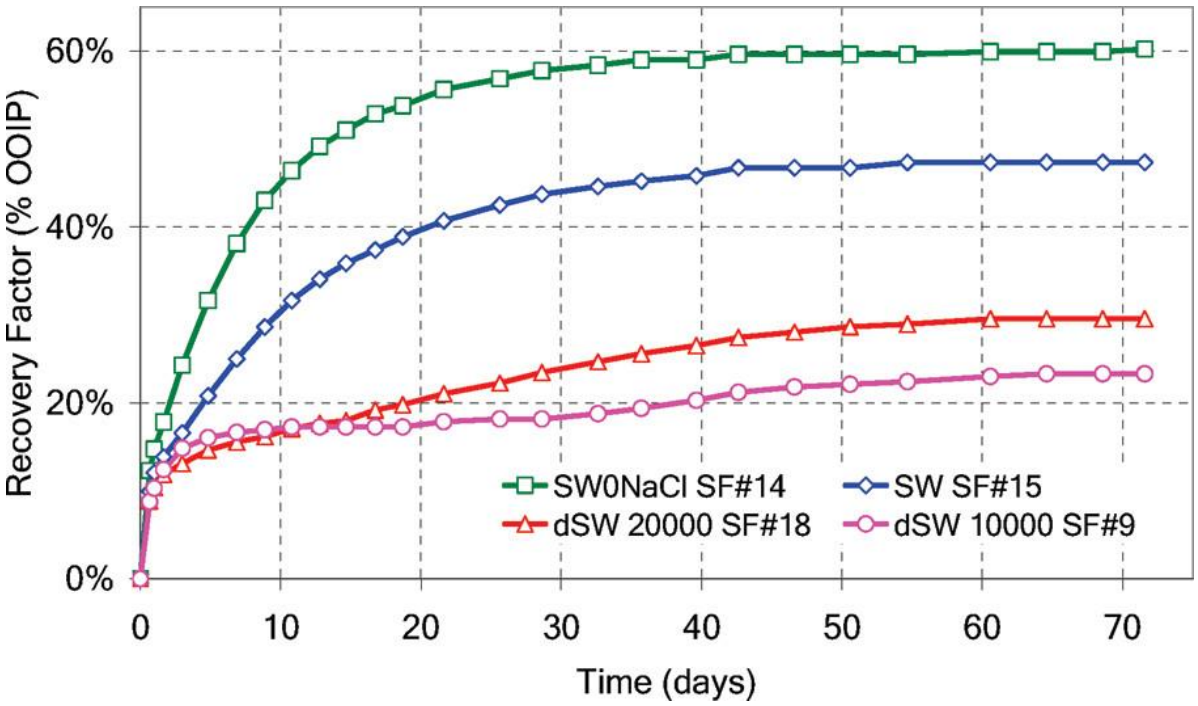

Figure 9. The Graph of Recovery Factor Over Time (Fathi et al., 2010)

2.6. Machine Learning Models

Support Vector Regression (SVR):

Support Vector Machines (SVM) are a class of supervised learning algorithms that are used for both classification and regression tasks and are grounded in the principles of statistical learning theory (Vapnik, 2000). A specialized version for regression problems, namely Support Vector Regression (SVR), is tailored to predict continuous outcomes. Similar to its classification counterpart, SVR is based on the concept of maximizing the margin, but instead of separating classes, SVR seeks to fit a function within a specified margin of tolerance (epsilon) around the actual data points (Suykens & Vandewalle, 1999). The model attempts to find a hyperplane in a high-dimensional space that best approximates the underlying data, allowing for a certain degree of error while penalizing deviations that fall outside the margin (Smola & Schölkopf, 2004). Only the data points that lie outside this margin (known as support vectors) influence the final model. In simpler terms, SVR can be viewed as drawing a “tube” around the regression function such that most training data lie within it, thereby balancing prediction accuracy and model simplicity. The SVR is particularly useful in capturing nonlinear relationships due to its flexibility in using various kernel functions,

including linear, polynomial, radial basis function (RBF), and sigmoid kernels (Cristianini & Shawe-Taylor, 2000). A schematic representation of the SVR is shown in Figure 10.

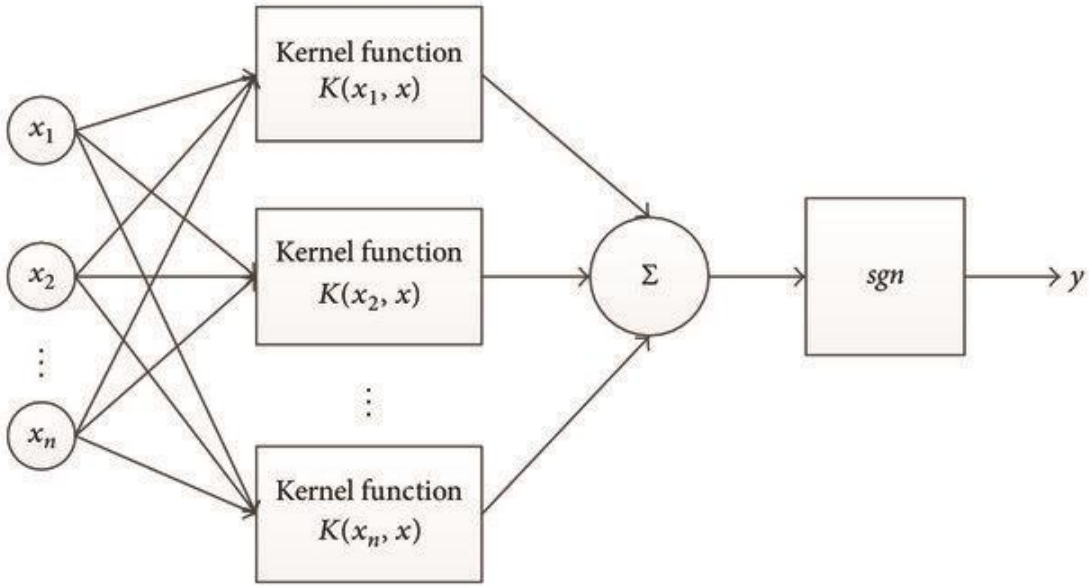

Figure 10. Schematic representation of the SVR model (Wang & Xu, 2017)

Decision Tree (DT):

Decision trees are a fundamental machine learning tool that is effective for classification and regression tasks, especially with tabular data. The core idea behind a decision tree is to learn a series of simple decision rules from the input features to predict a target variable (Loh, 2011). This is achieved by recursively partitioning the data into subsets based on the feature values that best separate the target variable. In the regression case, for each tree node, the algorithm selects a feature and threshold that produce the greatest reduction in variance. This process continues until the data are split into pure or nearly pure leaf nodes.

One of the key strengths of this supervised learning method is its ability to capture complex, nonlinear relationships in the data without requiring transformation or prior knowledge of the feature interactions. Unlike linear models, such as SVMs (without kernels), decision trees naturally model interactions and nonlinearities by structure (Loh, 2011). However, despite their easy interpretability and computational effectiveness, decision trees are susceptible to overfitting when grown deep. The methods focused on ensemble learning can be used to address this issue. A schematic representation of the DT is shown in Figure 11.

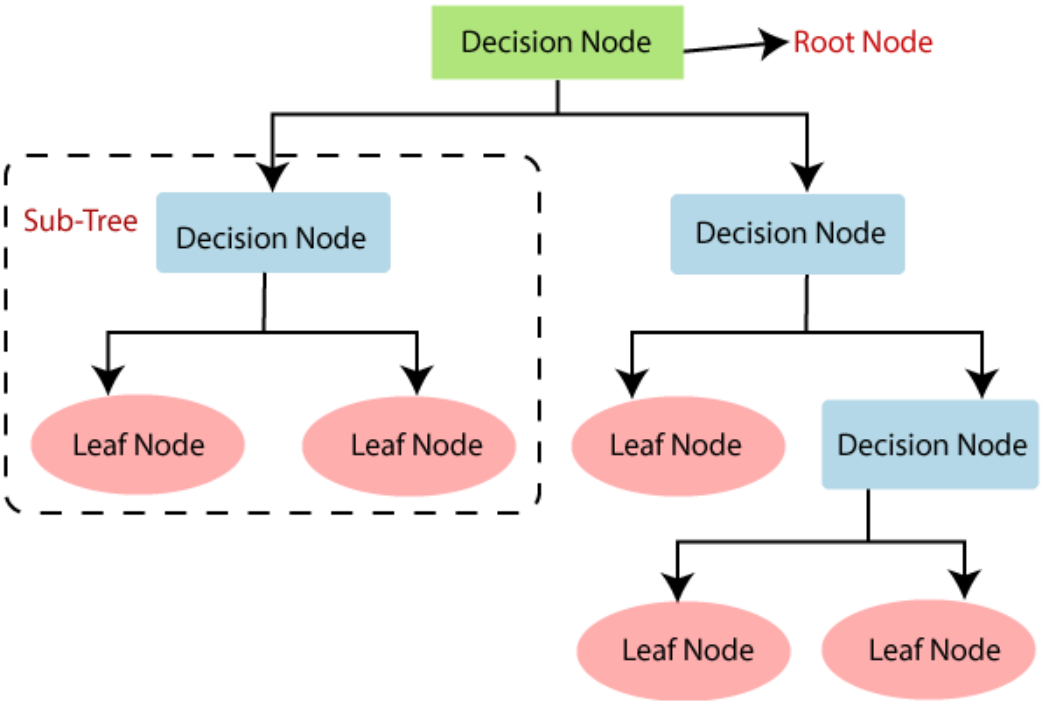

Figure 11. Schematic representation of the DT model (Komarasamy & Ravishankar, 2022)

Random Forest (RF): The RF is an ensemble learning method that combines predictions from multiple decision trees to improve performance and overcome overfitting (Breiman, 2001). Each tree was built on a bootstrap sample (a randomly drawn subset) of the training data, and only a random subset of features was considered when splitting nodes (Breiman, 1996). By averaging the predictions for the regression task across all trees, the random forest algorithm typically achieves better generalization than a single decision tree and is often overfitting-resistant. While individual decision trees can suffer from high variance (overfitting), combining many decision trees reduces variance without substantially increasing bias. This inherent randomness helps the model capture complex patterns without the need for intensive parameter tuning.

A schematic representation of the RF is shown in Figure 12.

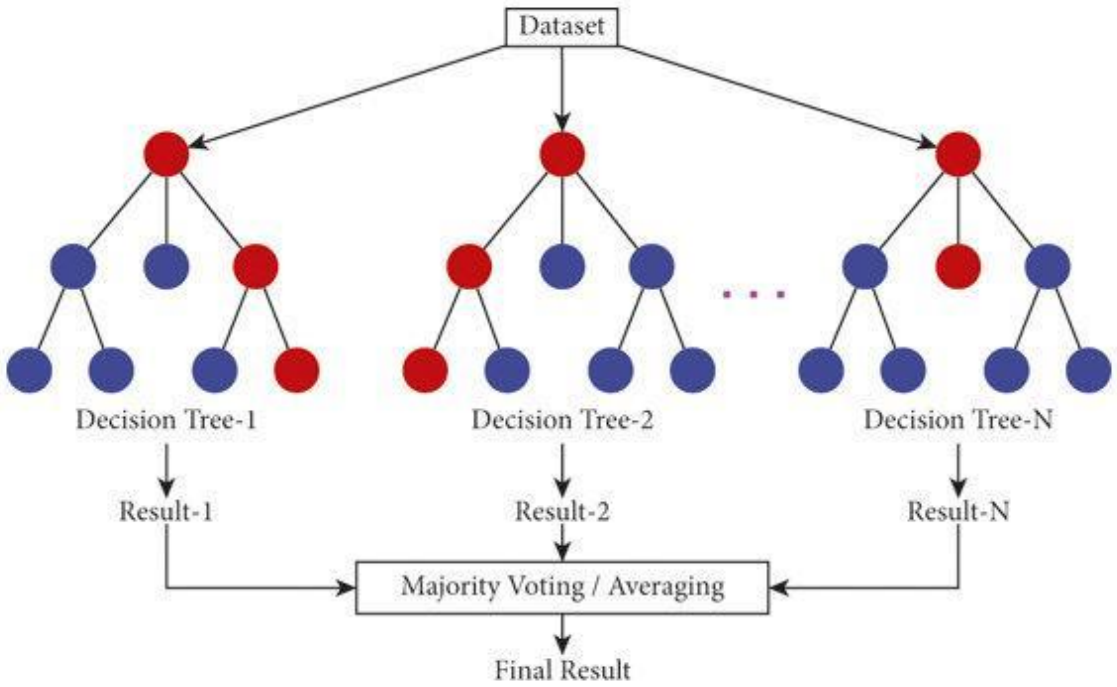

Figure 12. Schematic representation of the RF model (Khan et al., 2021)

Gradient Boosting (GB):

Gradient Boosting is an ensemble learning method that is widely used in both classification and regression tasks. It works by iteratively training new "weak" models (often decision trees) to correct the errors made by the existing ensemble (Friedman, 2001). At each iteration, the algorithm computes the gradient of a chosen loss function (e.g., mean squared error or cross-entropy) concerning the current predictions and fits a new model to these residual errors. The predictions of this new model are then added to the ensemble. Gradient Boosting effectively "boosts" accuracy in a stagewise manner by focusing on the biggest mistakes in each round. This results in higher performance compared to simpler methods like decision trees, and enables the widespread use of this technique, especially in scenarios involving high-dimensional or noisy data.

A schematic representation of the GB is shown in Figure 13.

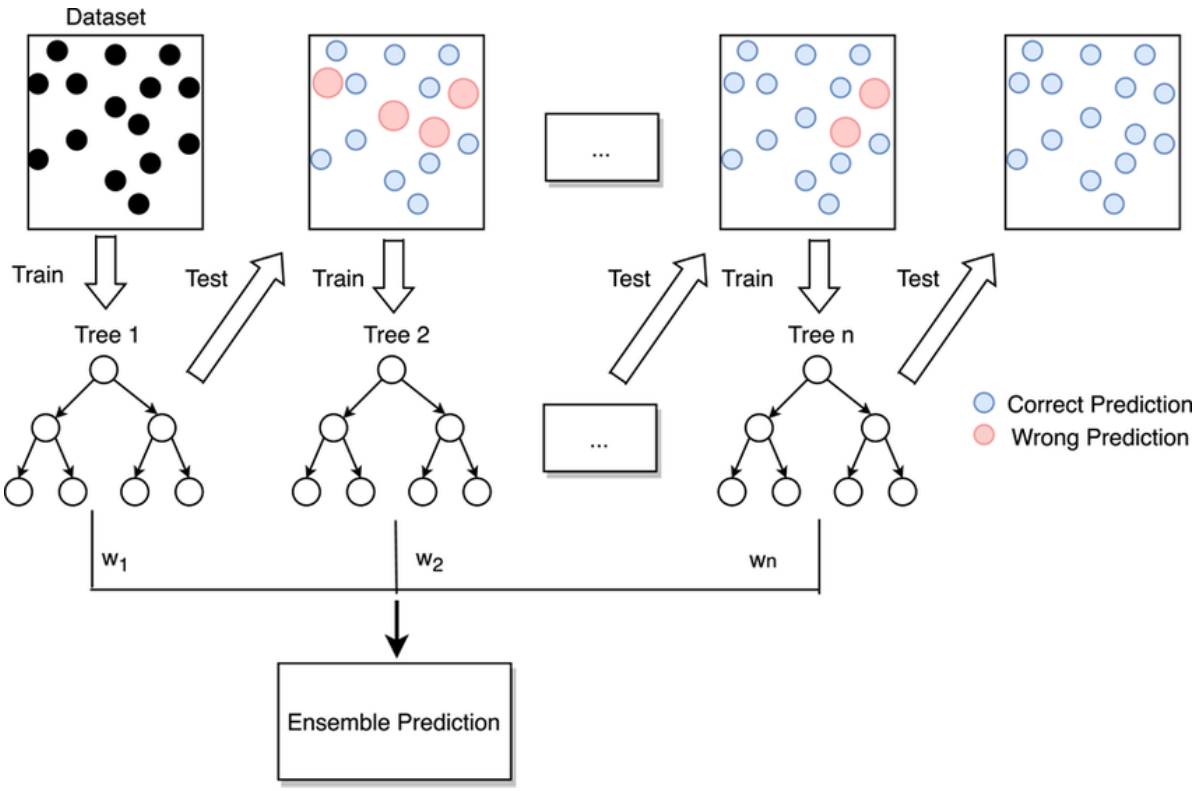

Figure 13. Schematic representation of the GB model (Zhang et al., 2021)

Extreme Gradient Boosting (XGBoost):

XGBoost is a high-performance gradient boosting framework that builds an ensemble of decision trees in a stagewise manner to optimize a differentiable loss function (Chen & Guestrin, 2016). Building on foundational work by Friedman (Friedman, 2001), it employs specialized techniques, such as sparsity-aware splits and a weighted quantile sketch, for efficiently handling large and sparse datasets (Chen & Guestrin, 2016). Additionally, XGBoost integrates regularization terms (e.g., L1 and L2 penalties) into its objective function to reduce overfitting and enhance model generalization. XGBoost can scale to large datasets while still offering rapid training speeds due to its parallelization and distributed computing capabilities.

A schematic representation of the XGB is shown in Figure 14.

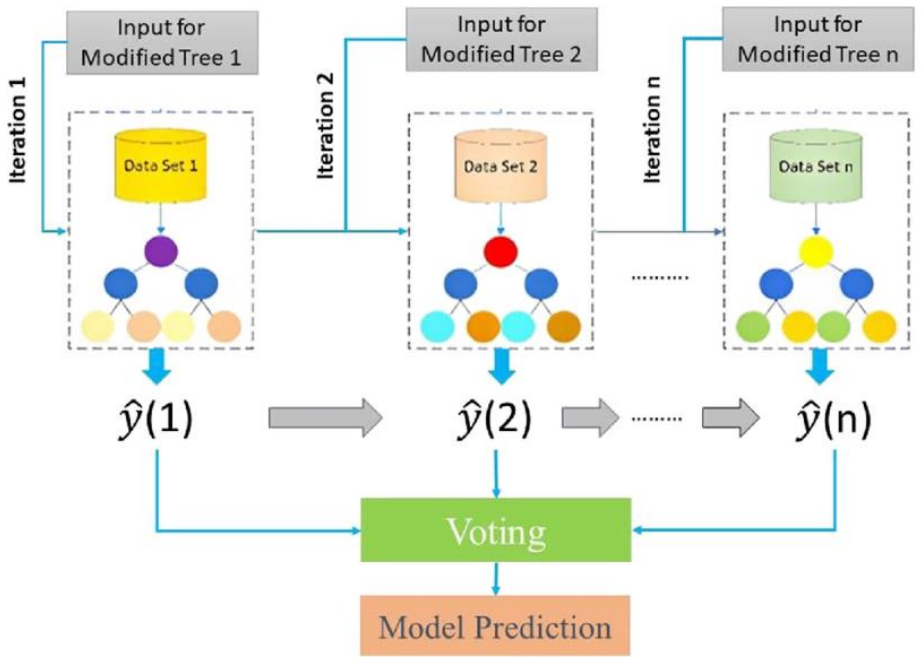

Figure 14. Schematic representation of the XGB model (Faska et al., 2023)

Artificial Neural Network (ANN):

A multilayer perceptron, also referred to simply as an artificial neural network (ANN), is a feedforward computational model that consists of interconnected layers of nodes: an input layer, one or more hidden layers, and an output layer (Bishop, 1995). Each neuron is tasked with computing the weighted sum of its inputs, followed by applying a nonlinear activation function (commonly ReLU, sigmoid, or tanh). Including nonlinear activation functions allows the network to capture complex nonlinear relationships in the data (Rumelhart et al., 1986). During training, the network gradually refines its internal parameters (weights and biases) using backpropagation, which measures the difference between predicted and actual values and propagates this error backward through the layers. By computing gradients at each layer, the network updates its parameters in the direction that reduces the overall loss (which is opposite to the direction of the gradient). This process is typically coupled with optimization techniques (i.e., Stochastic Gradient Descent (SGD), Adam, AdamW), which are used to guide the ANN toward an optimal solution represented as a global minimum in the loss landscape (Bishop, 1995). As a result, ANNs can learn rich hierarchical representations of data and thus achieve better performance than classical machine learning methods (Goodfellow et al., 2016). A schematic of the ANN is shown in Figure 15.

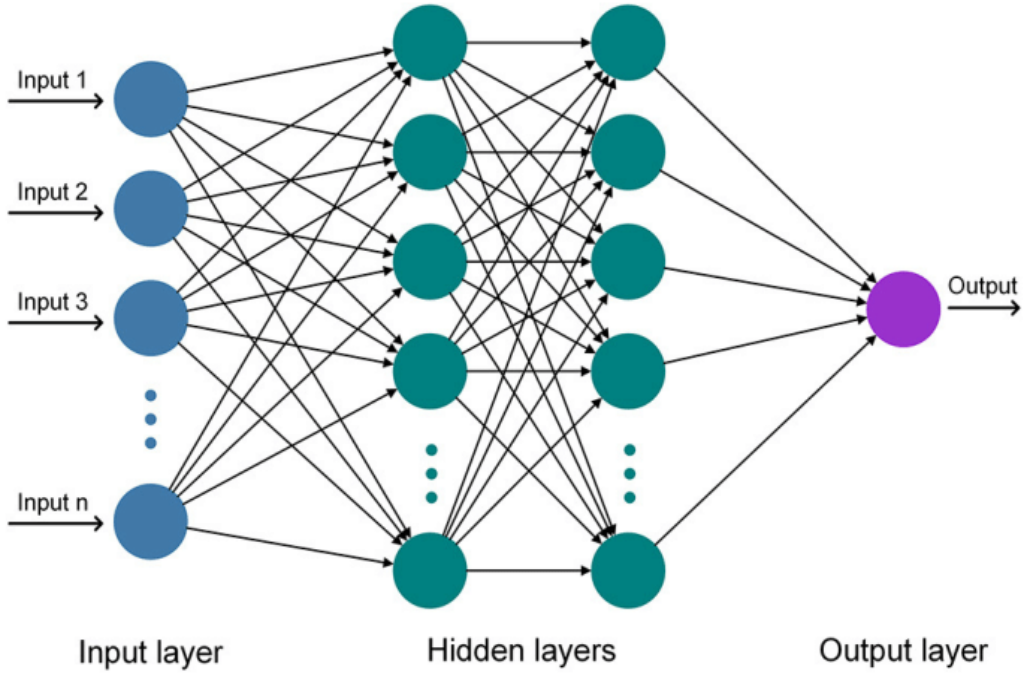

Figure 15. Schematic representation of an ANN (Sahraei et al., 2021)

2.7. Problem Statement

The spontaneous imbibition recovery obtained from LSW takes a lot of time and can be easily affected by external factors, making some results unreliable. In other words, having a machine learning model based on previously obtained results is an effective way to determine the precise and accurate effect of LSW on imbibition oil recovery without the need to conduct full-scale laboratory experiments.

The problem is that the application of machine learning methods to predicting LSW absolute spontaneous imbibition recovery is far from being completely investigated. There are still many gaps and possible applications of different machine learning methods, which can be studied. Therefore, there is still a lot of potential work that can be done in the field of machine learning methods. The present work investigates the effect of LSW on spontaneous imbibition oil recovery prediction. Such machine learning methods as Artificial Neural Networks, Decision Tree, Gradient Boosting, Random Forest, Support Vector Machine, and Extreme Gradient Boosting have been applied to predict spontaneous imbibition oil recovery. The performance of the models was analyzed on different datasets, and the best-performing model for each dataset was identified.

Chapter 3: Methodology

This research aims to predict the spontaneous imbibition of absolute oil recovery using different machine learning models. Thus, the methodology that was followed to predict the results of spontaneous imbibition is discussed in this section. The methodology comprises three parts: data gathering, data preprocessing, and data processing.

3.1 Data Gathering

Machine learning models predict results based on the data used to train and test the models. Obtaining an appropriate experimental dataset for the models to predict the spontaneous imbibition absolute oil recovery is a challenge. Each research paper is conducted on a different topic, and it is difficult to find enough data for LSW spontaneous imbibition experiments; moreover, it becomes challenging to group all of them and find similar properties to expand the dataset for the models. For this purpose, the set of frequently used parameters was selected to gather as much data as possible. Therefore, data from 25 research papers were gathered, and 395 spontaneous imbibition experiments were collected.

- Inputs of the model:
    1. Lithology;
    2. Length of the core (L);
    3. The diameter of the core (D);
    4. Porosity of the core (Φ);
    5. Initial water saturation of the core (Swi);
    6. Salinity of the brine;
    7. Temperature of the experiment (T).
- Output of the model:
    1. Recovery factor (RF).

The length parameter's significance primarily relates to gravity effects during spontaneous imbibition. In longer core samples, gravitational forces can influence fluid distribution and the oil-water front movement. Consequently, longer samples can experience varying oil recovery outcomes depending on their orientation and the dominance of gravitational forces relative to capillary forces. This parameter should be carefully evaluated to ensure its appropriateness for accurately representing the gravity influence on spontaneous imbibition recovery.

The diameter of the core sample influences boundary conditions during spontaneous imbibition experiments. Larger diameters minimize boundary effects due to a more significant central region, where edge influences are negligible. Conversely, smaller-diameter cores experience pronounced boundary conditions, potentially skewing results due to increased surface-to-volume ratios. Therefore, it is important to consider that factor.

Porosity affects spontaneous imbibition, as it directly relates to pore size distribution, impacting capillary pressure. Utilizing Leverett's J-function to characterize porosity effectively captures the pore-scale interactions within porous media. This approach incorporates porosity into a dimensionless parameter, making it suitable for generalizing and comparing imbibition results across different rock types and conditions. Porosity directly reflects the pore geometry and thus influences capillary action and fluid flow behavior crucial for accurate predictive modeling.

Lithologies were categorized into 3 types: chalk, sandstone and carbonate. The lithology types were used as input for the models in a numerical form, so that it covers these three rock types.

Initial water saturation (Swi) indirectly indicates the rock's wettability. Lower Swi values typically suggest less water-wet conditions, indicating the reservoir is less water-wet. Thus, Swi indirectly influences spontaneous imbibition by indicating wettability conditions, which fundamentally govern capillary pressure and fluid distribution within the porous medium. Recognizing Swi as a proxy for wettability can enhance predictive modeling accuracy by incorporating the wettability impact indirectly into spontaneous imbibition recovery forecasts.

Although the industry generally defines low-salinity water as having a salinity below 10,000 ppm, this study included a wider salinity range for comprehensiveness. In the analysis phase, emphasis is placed on how varying salinity affects oil recovery, with particular attention paid to recovery trends in the lower salinity range. The inclusion of data with higher salinities ensures model robustness and facilitates exploration of thresholds beyond which the benefits of LSW may diminish.

Temperature?

Table 2 summarizes the papers used in the machine learning models.

Table 2. Summary of the papers used for the machine learning models.

Referenc	Lithology	L (cm)	D	Φ (%)	Swi	Salinity	T (°C)	RF (%)	Data

e			(cm)		(%)	(ppm)			points
Fathi et al. (2010)	Chalk	6.92-7	3.78 - 3.81	45-47	8-9	1671 - 103648	100 - 120	14.4 - 69.3	12
Ravari (2011)	Limestone	5.01 - 6.13	3.79 - 3.84	12.8 - 17.4	10	33428 - 62901	25 - 130	5 - 38	10
Fathi et al. (2011)	Chalk	7	3.8	44 - 48	9-11	10021 - 62871	70 - 120	11 - 62	13
Roostaei (2014)	Carbonate Chalk	6.5 - 7.1	3.71 - 3.88	11 - 43	10	1668 - 138058	65 - 100	5 - 58.2	9
Romanuka et al. (2012)	Carbonate Chalk	5.08	3.81	12-51	10 - 17	941 - 222443	60 - 120	0.8 - 53.8	63
Sohrabi et al. (2017)	Sandstone	12.45 - 12.84	2.43 - 2.49	28.99 - 29.51	25.4 - 28.9	500 - 100000	60	4.3 - 13.4	3
Fathi et al. (2011)	Chalk	7.02 - 7.06	3.8 - 3.81	44-45	10-11	33438 - 62871	110	13.7 - 51.4	8
Fathi et al. (2010)	Chalk	6.93 - 7.1	3.8- 3.81	44- 46	9	33438 - 62871	110	14.8 - 57.4	8
Zhang et al. (2006)	Chalk	4.85 - 6.41	3.5- 3.75	47.2 - 50.3	0-9.2	30935 - 34239	70 - 130	17.5 - 67.3	22
Shehata et al. (2017)	Sandstone	7.112	3.81	18.6 - 20.5	37.3 - 46.8	5000	25 - 65	20.2 - 69	9
Shariatpanahi et al. (2010)	Carbonate	7.11 - 8.22	3.79 - 3.8	15- 17	10	11493 - 209178	110 - 130	38 - 54	10
Yang et al. (2016)	Sandstone	6.97 - 7.04	3.8 - 3.82	21.41- 21.73	25- 25.3	1000 - 39500	60	24.1 - 33.1	8
Mahzari et al. (2019)	Sandstone	7.45 - 14.85	2.53 - 3.78	20.96- 28	9.9 - 15.8	80000	80	3.3 - 18.9	12
Al-	Carbonate	4.6 -	3.8	22.4-	10.5 -	1944 -	70	9 - 27.9	12

Harrasi et al. (2012)		4.9		26.4	14.7	194450			
Nasralla et al. (2018)	Carbonate	5.007 - 5.02	3.8 - 3.81	15.7 - 25.3	10 - 15	4370 - 239400	70	2.7 - 23.6	33
Zaeri et al. (2018)	Carbonate	4.4 1 - 4.98	3.8	19.14 - 20.05	10	731.5 - 5852	35-75	3.1 - 13.9	6
Zaeri et al. (2019)	Carbonate	4.59 - 4.98	3.8	17.25 - 19.5	0-33	4148.1 - 8296.2	75	12.3 - 28.4	5
Feldmann et al. (2020)	Carbonate	5.08	3.81	15	24.5-32.9	438.5 - 183609	70	1 - 36.1	12
Strand et al. (2008)	Chalk	6.5	3.8	43.7 - 47.1	10	33428 - 62901	90-120	8 - 30.7	9
Puntervold et al. (2009)	Chalk	6.5	3.8	44.9 - 49.6	8.3 - 9.5	36932 - 65034	50-130	27.2 - 67.3	23
Mehraban et al. (2020)	Carbonate	7.134 - 7.62	3.82	17.56 - 18.98	30.2 - 40.1	48088 - 66625	90	34.89 - 43.54	4
Nowrouzi et al. (2019)	Carbonate	6.98 - 7.11	3.82	19.89 - 25.19	8.22 - 33.42	1000 - 10500	75	30 - 65.6	6
Gachuz-Muro et al. (2014)	Carbonate	9.7 - 15.3	2.5 - 2.64	20.79 - 37.42	28.78 - 37.42	37167.6	92	14 - 16.4	4
Sorop et al. (2015)	Sandstone	5.08	3.81	28	1-10	1500 - 265608	45	2.5 - 30	4
Suijkerbuijk et al. (2012)	Sandstone	5.08	3.81	8.2 - 22.5	5-20	240 - 237858	60 - 70	22.1 - 74.2	90
								Total:	395

Table 2 presents the datasets for both the secondary and tertiary datasets. This dataset was further subdivided into two smaller datasets: secondary and tertiary. The statistical analysis results for the three datasets are shown in Tables 3, 4, and 5.

Table 3. Statistical Summary of the Secondary Dataset

	L (cm)	D (cm)	Φ (%)	Salinity (ppm)	T (°C)	RF (%)
Mean	7.04	3.70	32.74	37269.68	83.94	30.59
Median	6.50	3.80	28.50	33433.00	75.00	32.00
Std Dev	2.68	0.30	14.18	38459.79	26.51	19.09
Min	4.41	2.43	9.70	438.50	25.00	1.00
Max	15.30	3.88	50.30	239400.00	130.00	69.34

Table 4. Statistical Summary of the Tertiary Dataset

	Swi (%)	Salinity (ppm)	T (°C)	RF (%)
Mean	13.13	58051.02	75.54	33.40
Median	12.00	25578.00	70.00	30.45
Std Dev	4.18	79660.32	18.55	22.95
Min	1.00	240.00	45.00	0.84
Max	25.30	265608.00	120.00	74.15

Table 5. Statistical Summary of Both the Secondary and Tertiary Datasets

	L (cm)	D (cm)	Φ (%)	Swi (%)	Salinity (ppm)	T (°C)	RF (%)
Mean	6.09	3.76	27.18	14.47	49528.04	78.98	32.25
Median	5.08	3.81	22.10	12.00	25578.00	70.00	31.25
Std Dev	1.99	0.20	12.14	7.68	66676.56	22.51	21.47
Min	4.41	2.43	4.40	0.00	240.00	25.00	0.84
Max	15.30	3.88	51.00	46.80	265608.0	130.0	74.15

3.2 Data Preprocessing

3.2.1 Box Plots

Box plots provide valuable insight into the distribution of data points across a selected feature, primarily information about a group of data's symmetry, skew, variance, and outliers. The box plots for each data feature for each dataset are shown in Figures 16, 17, and 18.

Across all datasets, Salinity exhibited the widest spread and most extreme outliers. This indicates significant environmental variation, especially in the Combined dataset, where the salinity values exceeded 250,000. Such values were excluded and considered as outliers. Porosity (Φ, %) showed a broad distribution in the Combined and Secondary spontaneous imbibition datasets, with values ranging from less than 10% to nearly 50%, reflecting diverse rock properties. Initial water saturation (Swi%), in turn, displayed a wide range of frequent outliers (particularly in the Combined dataset). However, Swi in the Secondary spontaneous imbibition data had a tighter distribution, suggesting greater consistency. Core dimensions, specifically core diameter (D), remained tightly clustered across all datasets, whereas core length (L) exhibited moderate variability. Temperature (T, °C) predominantly centered between 60 and 80 °C, with a few outliers extending beyond 120 °C.

To summarize, the Combined dataset showed the highest variability compared with the secondary and tertiary spontaneous imbibition datasets, which exhibited more consistent internal distributions.

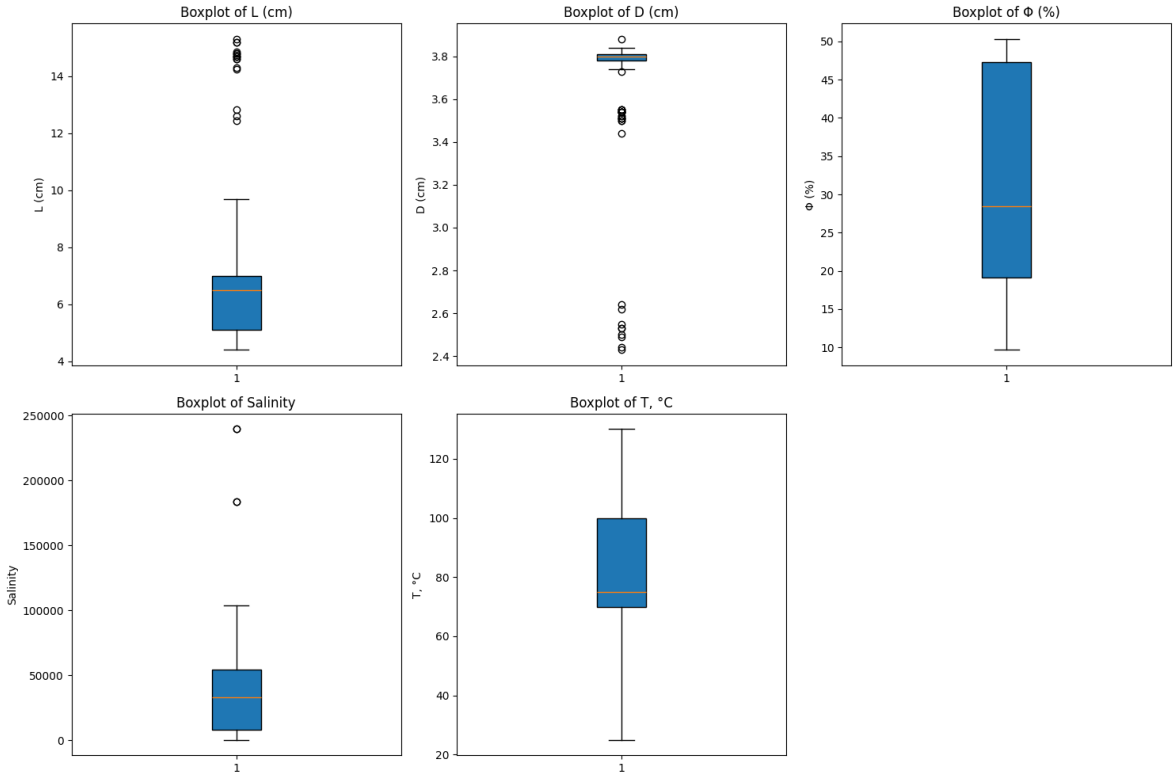

Figure 16. Box Plots for Secondary Dataset

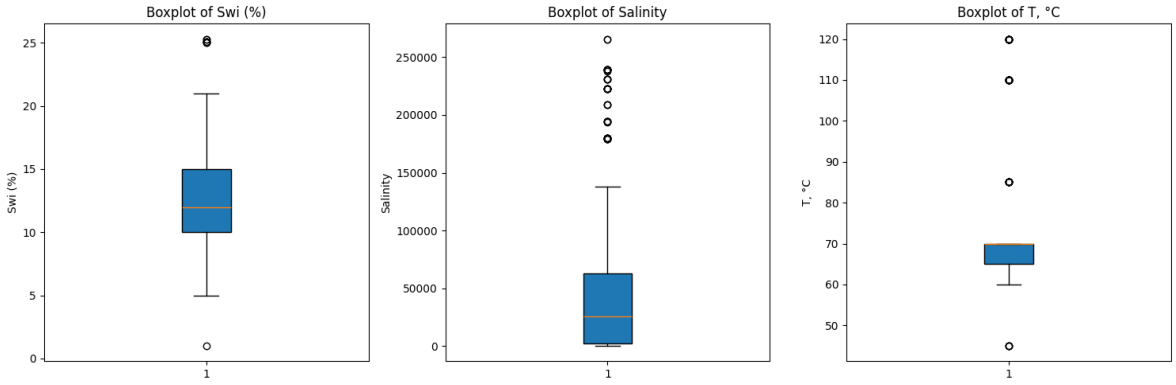

Figure 17. Box Plots of Tertiary Dataset

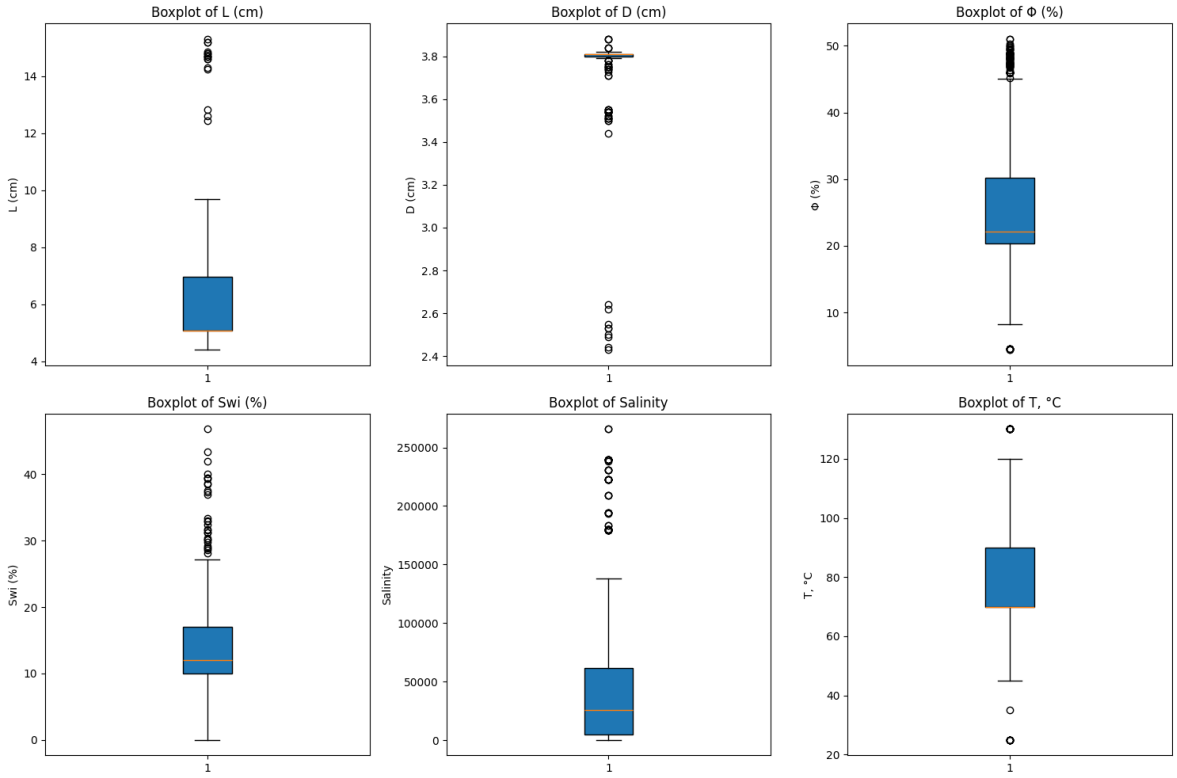

Figure 18. Box Plots for Secondary and Tertiary Datasets

After analyzing the box plots presented in Figures 16, 17, and 18, it can be seen that there are many outliers in each input parameter. Thus, it was decided to eliminate outliers. Outliers are any point that lies beyond the 25-75% margin. In this way, the models could train and test data without noise.

3.2.2 Pair Plots

Pair plots are useful for visualizing pairwise relationships in datasets. In this section, we provide pair plots for each dataset before and after removing the outliers to visualize the effectiveness of the proposed data preprocessing strategy.

In Figures 19, 20, and 21, we provide the pair plots for the raw dataset without preprocessing. In all three datasets, extreme values in features like Salinity and Swi (%) introduced heavy skewness in the distributions and densely stacked scatter points, which made it difficult for the models to comprehend potential patterns between input features and the target variable.

Although lithology-based grouping remains somewhat visible (especially for RF), this separation is visually diluted in the presence of outliers.

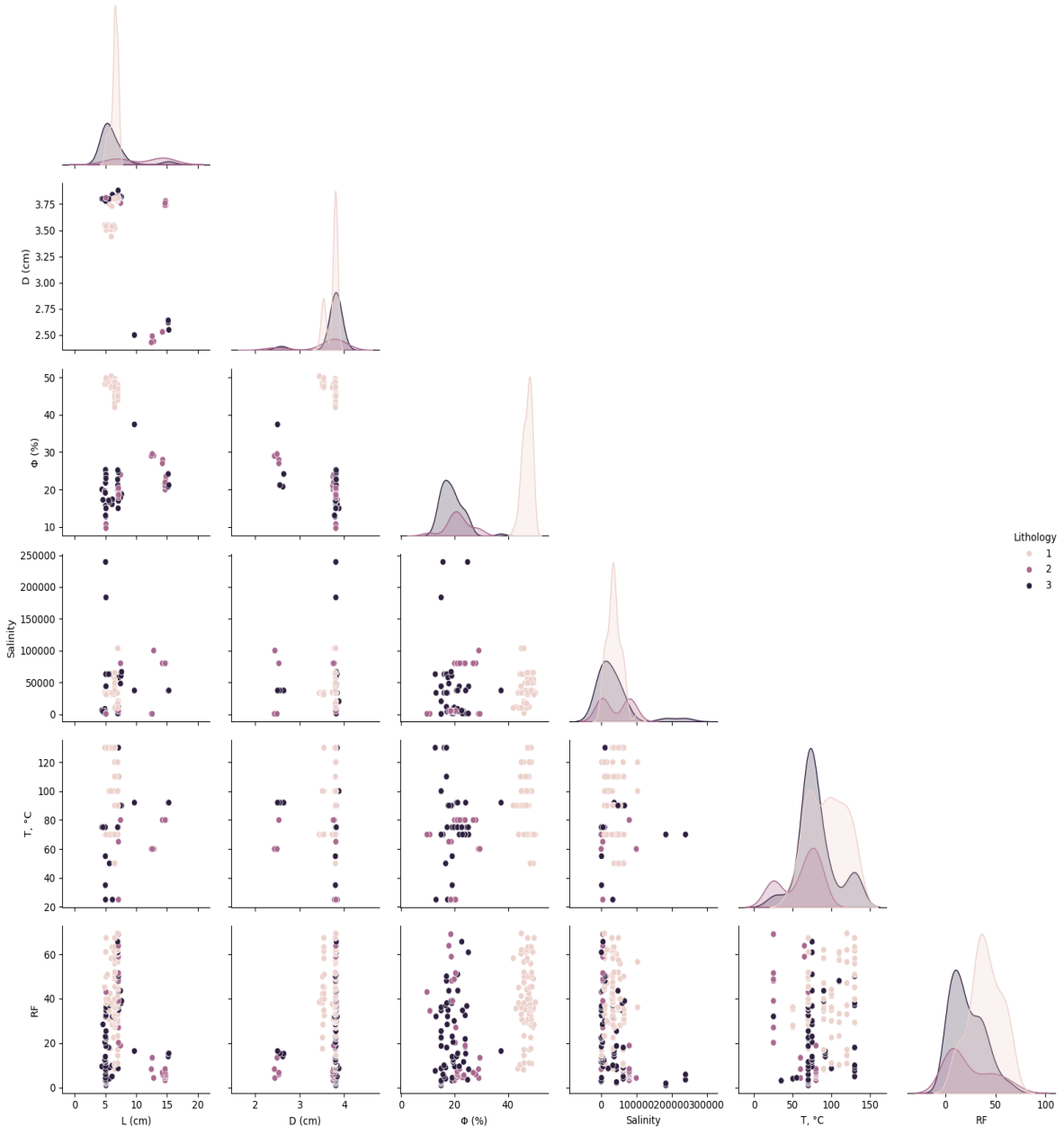

Figure 19. Pair Plot showing Dependencies between Parameters of Secondary Dataset Before Cleaning

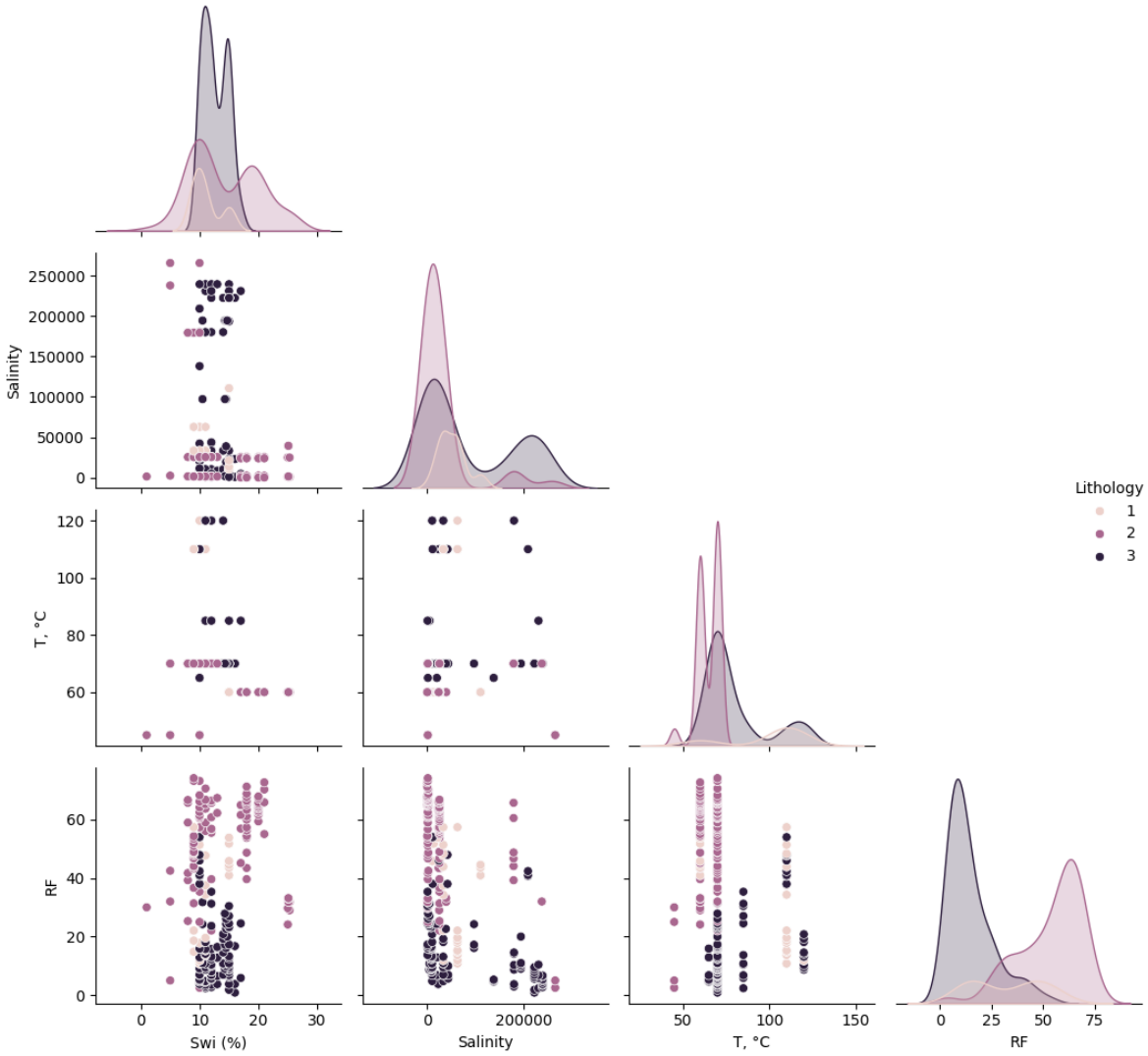

Figure 20. Pair Plot showing Dependencies between Parameters of Tertiary Dataset Before Cleaning

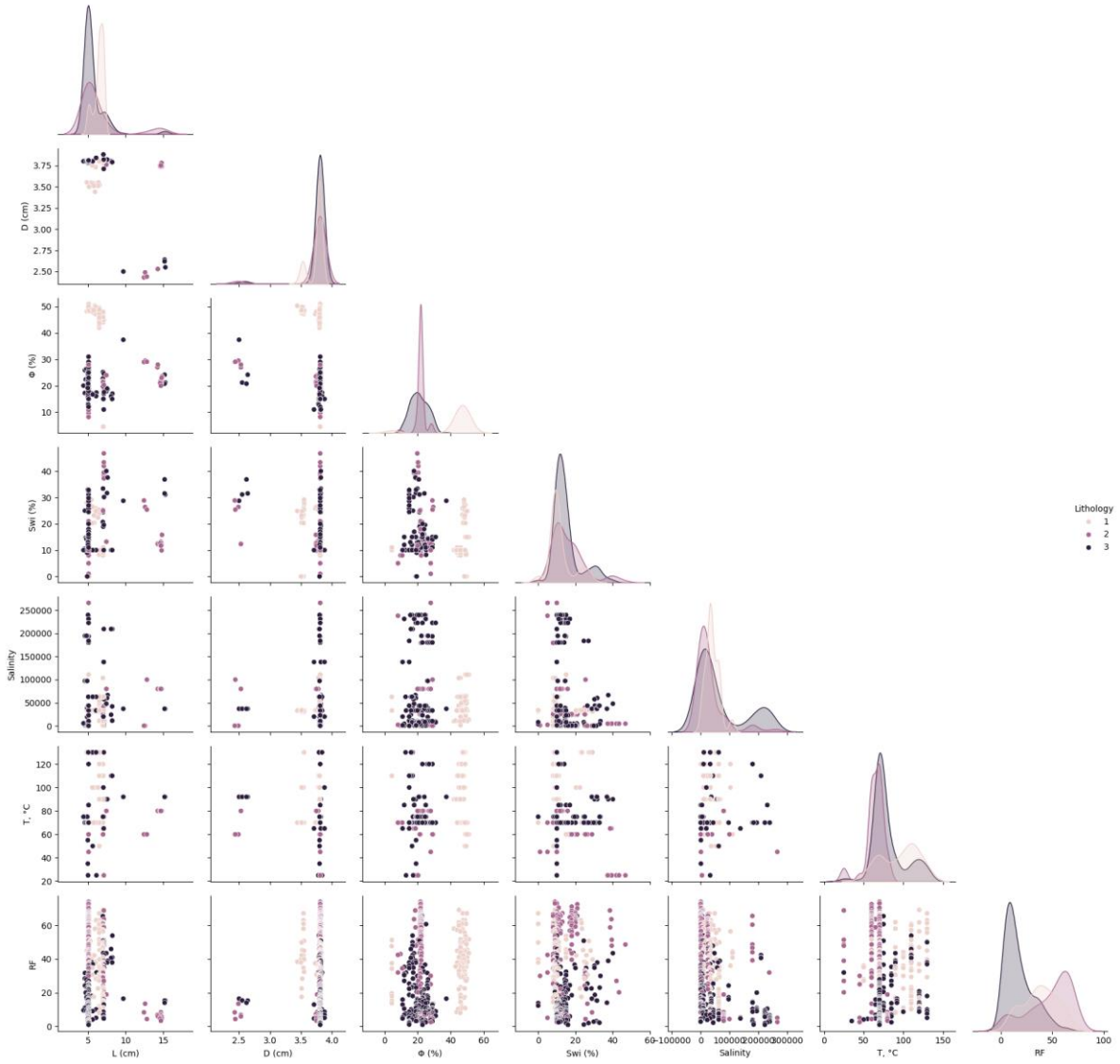

Figure 21. Pair Plot showing Dependencies between Parameters for Secondary and Tertiary Datasets Before Cleaning

The pair plots after outlier removal are shown in Figures 22, 23, and 24. In the Tertiary Imbibition dataset, RF exhibited clear separation across the lithology classes, with Lithology 3 and Lithology 1 generally associated with higher and lower RF values, respectively. Similar patterns were observed in the Secondary Imbibition dataset, where features such as porosity (Φ%), initial water saturation (Swi%), and salinity notably varied across lithologies, suggesting that Lithology could serve as a useful categorical feature in RF prediction.

Across all datasets, RF exhibited meaningful relationships with several features. In particular, there is a visible trend of increasing RF with higher porosity and lower Swi, especially in the

Combined dataset. Features like core diameter (D) and temperature (T, °C), in turn, appear less informative with tightly clustered values. Notably, the combined dataset exhibited greater variability, which was probably due to the combined sources.

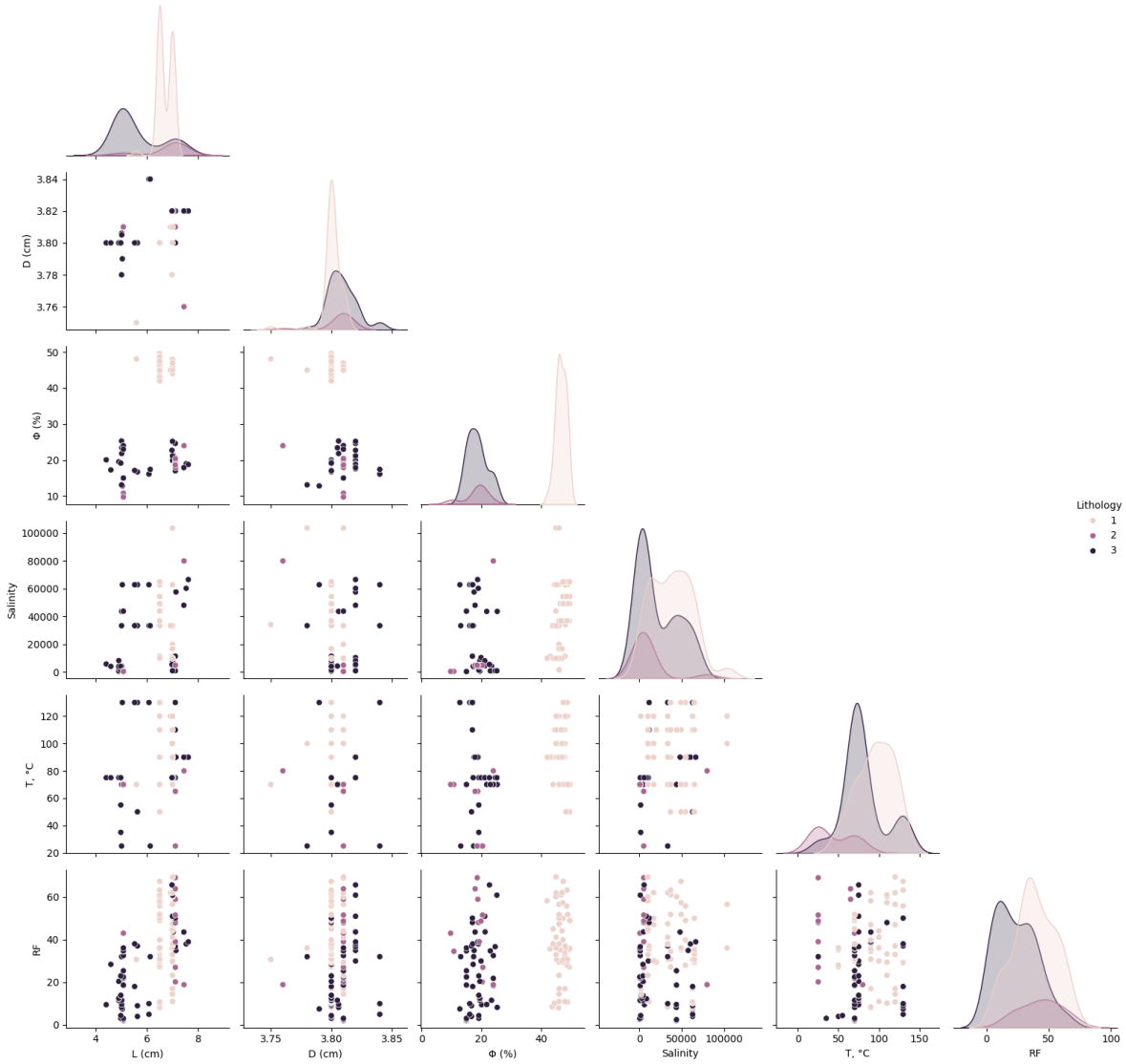

Figure 22. Pair Plot Showing Dependencies Between Parameters of Secondary Dataset After Cleaning

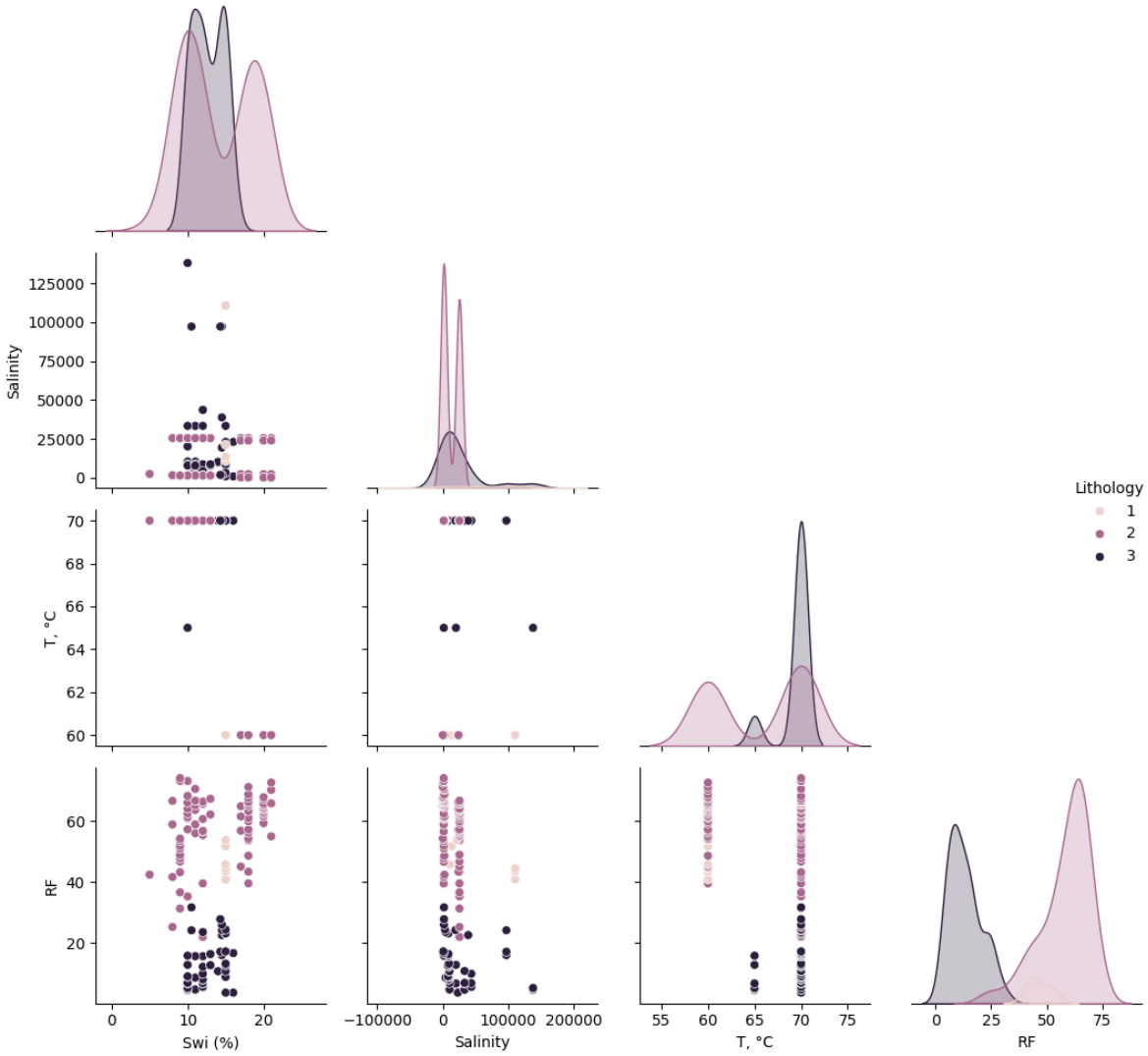

Figure 23. Pair Plot Showing Dependencies Between Parameters of Tertiary Dataset After Cleaning

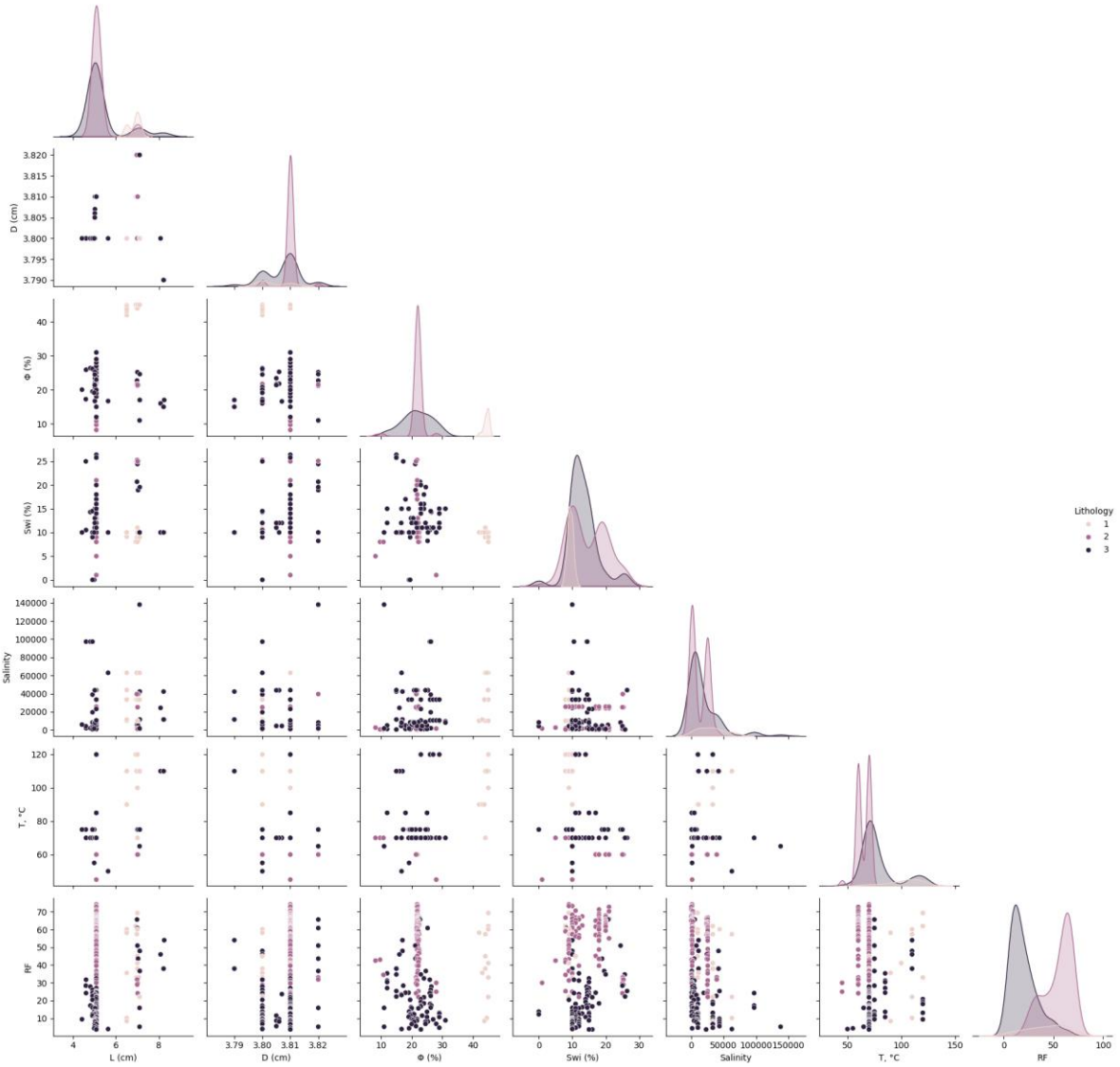

Figure 24. Pair Plot Showing Dependencies Between Parameters for Secondary and Tertiary Datasets After Cleaning

3.2.3 Heatmaps

The heatmaps present Pearson correlation coefficients between the input variables and target variables. Figures 25, 26, and 27 show heatmaps showing the correlation between the inputs and the recovery factor (RF) for all three datasets.

A common trend for all three datasets was that porosity (Φ, %) exhibits the strongest and most consistent positive correlation with RF, particularly in the secondary dataset (r = 0.43). This relationship indicates that porosity has a significant effect on recovery, which is in agreement with common practice.

Salinity, in turn, exhibits a negative correlation with RF across all datasets, with the most substantial negative relationship observed in the tertiary dataset (r = –0.45). This tendency aligns with the concept that the lower the water's salinity, the higher the recovery factor. Initial water saturation (Swi, %) and temperature (T, °C) showed moderate negative correlations with RF in the tertiary dataset, but these relationships were weaker or inconsistent in the combined and secondary datasets.

Core length (L) and core diameter (D) are minimally correlated with RF across all datasets. Correlations between other pairs of input features (e.g., Φ with T or Swi) remain weak, suggesting that these features have limited impact on each other.

The correlation matrix in the heatmaps indicates statistical associations, not necessarily physical causation. Correlations between core length and diameter arise due to sampling patterns in published datasets rather than underlying physical processes. Therefore, while useful for initial exploratory analysis, these correlations should be interpreted cautiously and not overestimated in terms of physical significance.

Figure 25. Heatmap for Secondary and Tertiary Datasets

Figure 26. Heat Map of Secondary Dataset

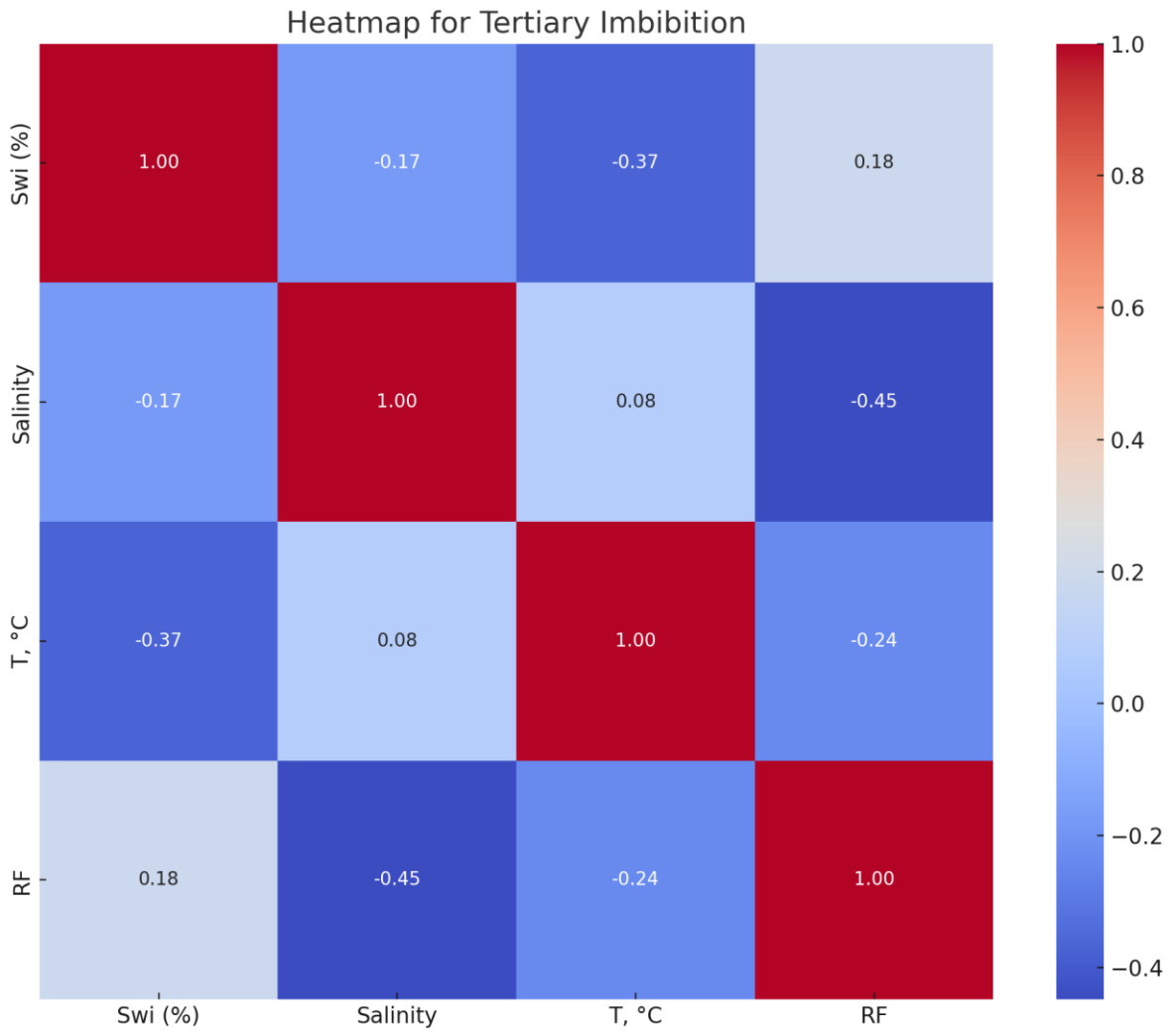

Figure 27. Heatmap of Tertiary Dataset

3.3 Data Processing

3.3.1 Model selection

In this thesis, the following methods were explored for predicting the recovery factor:

- **Support Vector Machine for Regression (SVR):**
  - A regression method focused on finding the hyperplane and function that effectively fit the data within a tolerance margin.
- **Decision Tree (DT):**
  - A method that splits data based on input features to minimize variance within each resulting subset by learning splitting decision rules.
- **Random Forest (RF):**

    - Ensemble learning method that creates multiple decision trees and makes the final prediction by averaging the outputs of the trees.
- **Gradient Boosting (GB):**
    - An ensemble learning method that iteratively trains weak learners in which each learner corrects the mistakes of its predecessor.
- **Extreme Gradient Boosting (XGBoost):**
    - Optimized gradient boosting with the incorporation of advanced regularization techniques
- **Artificial Neural Network (ANN):**
    - A deep learning method comprising multiple layers of neurons that learn to approximate complex functions from input data via training.

3.3.2 Test and training sets

To evaluate model performance, we employed an 80-20 train-test split. The collected dataset was randomly shuffled to prevent any bias resulting from the ordering and then divided such that 80% and 20 % of the data were used for training and testing, respectively. This approach allows us to preserve a substantial subset for testing and checking models' generalizability while retaining sufficiently large portions of data for training.

To further ensure the fairness of our evaluation setup, we performed a 5-fold validation. The dataset was split into 5 parts, and the models were trained on 4 parts and tested on the remaining part. This process was repeated 5 times, so each part was used once as the test set. The final performance was averaged across all 5 runs to ensure a more reliable estimate of the model's generalizability.

3.3.3 Tuning of Hyperparameters

The performance of the machine learning model can vary significantly depending on the hyperparameters that define the structure and function of the overall system. Therefore, it is essential to identify a hyperparameter set that yields optimal performance on the target data. To identify the most suitable hyperparameters for each machine learning algorithm, we employed a grid search. The proposed method exhaustively searches for the combination of hyperparameters that result in the highest performance. In our experimental setup, we selected the hyperparameter set that resulted in the highest R^2in the test set. The sets of hyperparameters produced by the grid search are summarized in Table 6.

Table 6. Summary of Hyperparameters of the Models

Model	Hyperparameter	Both	Secondary	Tertiary
ANN	Hidden layers Neurons Optimizer Batch size Epochs	10 8-1024 AdamW 32 500	10 8-1024 AdamW 16 500	5 8-128 Adam 32 500
DT	Max depth Min samples split Min samples leaf	4 8 1	2 2 1	6 6 1
GB	N estimators Max features Max depth Min samples split Min samples leaf	50 Sqrt 4 6 1	50 Sqrt 6 6 1	50 Sqrt 2 6 1
RF	N etimators Maximum features Maximum depth Samples split min Samples leaf min	200 Sqrt 8 8 1	50 Sqrt 10 4 1	200 Sqrt 4 8 1
SVM	C Kernel Epsilon Gamma	100 Rbf 0.0000001 0.01	10 Rbf 0.0000001 0.001	100 Rbf 0.0000001 0.01
XGB	N estimators Maximum depth Learning rate Minimum child weight	200 8 0.01 6	500 6 0.01 4	500 2 0.01 6

3.3.4 Model Evaluation

The model evaluation is based on several metrics:

1. Mean Absolute Percentage Error (MAPE):

This metric shows, on average, how far off our predictions are from the actual values. It is useful because it provides an intuitive sense of the prediction error in terms of percentage, which is easy to understand and compare across datasets (de Myttenaere et al., 2016).

$$MAPE = \frac{1}{n}\sum_{i=1}^{n}\left|\frac{x_{measured}-x_{pred}}{x_{measured}}\right| \quad (1)$$

2. Root mean square error (RMSE):

This metric measures the average difference between predicted and actual values, giving more weight to larger errors. It is great for spotting big mistakes because it penalizes large deviations more than small deviations (Willmott & Matsuura, 2005).

$$RMSE = \sqrt{\frac{1}{n}\sum_{i=1}^{n}(x_{measured} - x_{pred})^2} \quad (2)$$

3. R^2 Score:

R^2 shows how well the model explains the variability of the actual data. A value close to 1 indicates that the model's predictions are very close to real values. If it is 0, the model is not performing better than simply guessing the average (Kvålseth, 2017).

$$R^2 = 1 - \sum_{i=1}^{n}(x_{measured} - x_{pred})^2 / \sum_{i=1}^{n}(x_{measured} - x_{avr\ measured})^2 \quad (3)$$

4. Akaike Information Criterion (AIC):

AIC helps compare models by observing how well they fit the data while penalizing models for being too complex. A lower AIC means a better model—one that balances accuracy and simplicity (Vrieze, 2012).

$$AIC = -2\ ln(likelihood) + 2P_n \quad (4)$$

5. Bayesian Information Criterion (BIC):

Similar to AIC, BIC also balances fit and complexity; however, it applies a stronger penalty when adding additional parameters. It is especially useful when working with large datasets and avoiding overfitting (Neath & Cavanaugh, 2012).

$$BIC = -2\ ln(likelihood) + [ln(n)]P_n \quad (5)$$

These metrics were selected to properly evaluate the performance of the models to predict accurate and precise results.

Chapter 4: Results and Discussion

This section presents a comparative analysis of the performance of the models. The ANN, DT, GB, RF, SVM, and XGB machine learning models have been accomplished. This section presents the analysis of the prediction of secondary imbibition, tertiary imbibition, and both.

4.1 Application of Machine Learning Models to Secondary Imbibition

Table 7 summarizes the results. The models were trained and tested on the secondary imbibition dataset. The main metric on which the models are being compared is the R^2 for both training and testing. R^2_{train} shows how well the most optimized model fits the data after the model has trained itself multiple times based on the training data. R^2_{test} shows how well the trained and optimized model performs on unseen testing data. R^2 values close to 1 indicate very accurate fitting of the predicted and actual data. Based on training R^2, three models have $R^2_{train} > 0.8$, which are ANN, GB, and XGB. The highest training performance was achieved using the GB model, resulting in $R^2_{GB\ train}$=0.919. The ANN and XGB methods also demonstrated good performance, resulting in R^2_{train} values of 0.808 and 0.887, respectively. However, if we compare testing R^2, the performance of the models is completely different. R^2_{test} is more meaningful in our case because it demonstrates the usability of our models in real-world scenarios. If the R^2_{train} is high but the R^2_{test} is low, then the model overfits, meaning that it learns the noise rather than the real data patterns. Among all of the models, only two of them achieve R^2_{test} being more than 0.7, which are the GB and RF models. Although the $R^2_{RF\ train}$ is 0.788, the $R^2_{RF\ test}$ is 0.733, indicating only a 0.05 difference between the two metrics. However, the best performance by the R^2_{test} metric was achieved with GB, resulting in the $R^2_{GB\ test}$ having a performance of 0.748. This indicates that the model can accurately predict the secondary spontaneous imbibition recovery factor in almost 75% of cases.

Table 7. Models for Secondary Imbibition Tests

Parameter	ANN	DT	GB	RF	SVM	XGB
$MAPE_{train}$	52.603	63.981	32.880	13.229	77.039	39.444
$RMSE_{train}$	10.286	12.905	5.202	3.637	12.005	39.229
R^2_{train}	0.808	0.469	0.919	0.788	0.598	0.887

Parameter	ANN	DT	GB	RF	SVM	XGB
AIC_{train}	452.205	494.834	324.025	337.402	481.252	358.925
BIC_{train}	470.008	512.637	341.828	354.420	499.055	376.728
$MAPE_{test,}$	77.761	108.094	22.416	70.286	35.810	27.327
$RMSE_{test}$	13.885	16.312	12.569	16.331	15.256	160.539
R^2_{test}	0.543	0.288	**0.748**	0.733	0.504	0.627
AIC_{test}	140.278	148.012	135.500	190.759	144.800	135.884
BIC_{test}	148.525	156.258	143.746	199.553	153.046	144.131

In addition, other metrics that play more of a support role describe GB as the best model for this dataset. A value of $RMSE_{train}$ of 5.202 indicates that the GB model's predictions deviate by 5.2 units from the actual values during training. $RMSE_{test}$ of 12.569 shows an increase compared to the training value, meaning that the prediction deviates by approximately 12.5. On the other hand, $Mape_{train}$ equals 32.88%, meaning that the predictions deviate by over 33% from the actual values, and $Mape_{test}$ is 22.416%. Although the deviation by RMSE increased, the deviation by MAPE decreased. This could be occurring by the distribution of the data; thus, for the training part, the distribution is more toward the lower values, resulting in 5.2 deviation being 33.28%, and for the training part, the distribution is more toward the higher values, and 12.5 deviation results in 22.416%. The distributions of the data for the training and test sets are represented in Figure 28, where the red line represents an R^2 of 1. The distributions of the other machine learning models are shown in Figures 36-40.

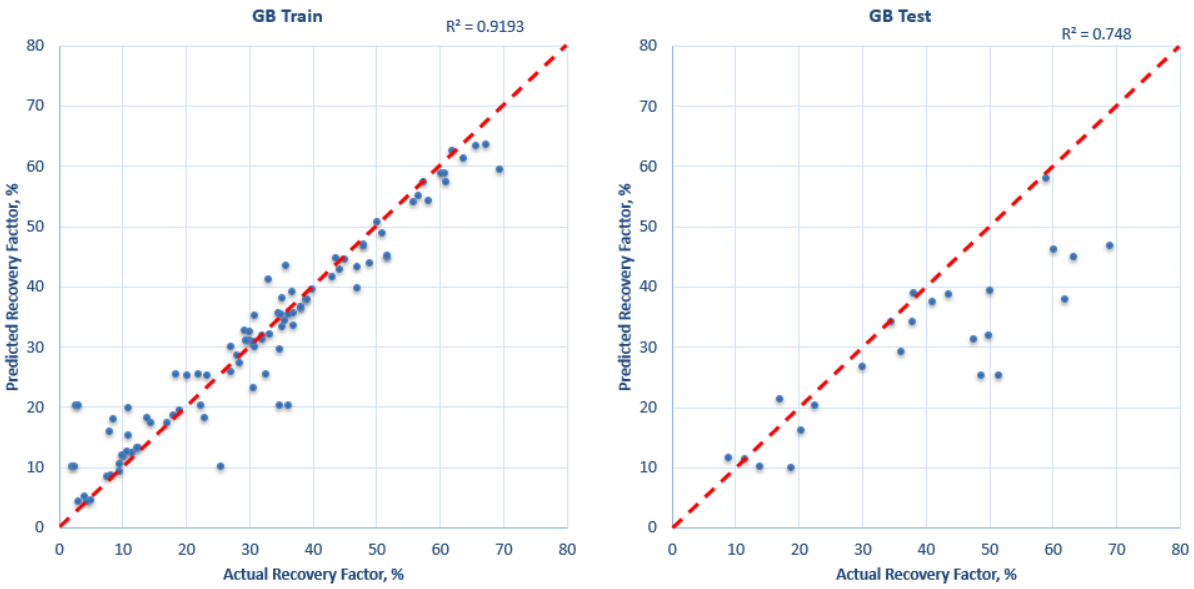

Figure 28. Results of R^2 for the GB Model for the Secondary Dataset

The AIC and BIC values also support the GB model. The lower these values are, the better the model can perform in terms of balance and result in minimum overfitting. For the training part, AIC_{train} is 324.025 and BIC_{train} is 341.828, which were the lowest values compared to the other machine learning models. For the testing part, AIC_{test} is 135.500 and BIC_{test} is 143.746, which were also the lowest values. The decrease between the training and testing parts was considerable, which demonstrates the improvement in the model's balance and decrease in the model's overfitting.

All metrics demonstrate that the proposed GB model is the best-performing machine learning model for secondary imbibition prediction. However, the prediction of 75% is still far from being completely reliable and accurate, and there is still a lot of room for improvement. Multiple possible causes affect the testing part of the model. The first possible reason is that the dataset itself is not that big, containing data from only 162 secondary imbibition experiments before cleaning and leaving only 118 experiments after the cleaning: 94 for training and 24 for testing. In other words, 24 data points for the testing part are not enough for the model to properly predict the results. The second reason is the quality of the data. The imbibition oil recovery is highly affected by the contact angle and IFT. The dataset does not contain this information because most of the research was done without measuring these properties. LSW increases imbibition oil recovery by altering these parameters, and the only input variable that somehow concerns the contact angle and IFT is salinity. Third, the values

of the recovery factors were extracted from the graphs using Plot Digitizer, which increases the human error. This could also affect model performance. The main problem was not in the models themselves but in the quality of the dataset.

4.2 Application of Machine Learning Models to Tertiary Imbibition

Table 8 summarizes the metrics obtained after predicting the models based on the tertiary spontaneous imbibition experiment data. By comparing the results from Tables 7 and 8, the models' performance based on tertiary imbibition data was better in all terms than that based on secondary imbibition data. All models resulted in R^2_{train} being greater than 0.9, meaning that the prediction of the training data was accurate for more than 90% of the cases. The highest R^2_{train} of 0.914 was achieved by the SVM model, and the lowest R^2_{train} of 0.901 was achieved by the ANN. All of the models' training R^2 are in the range of 0.901-0.914. But even the value R^2_{train} of 0.901 indicates high machine learning performance. In addition, the test results show no significant difference between R^2_{test} and R^2_{train}. The highest R^2_{test} of 0.896 was achieved by the RF model, and the lowest R^2_{test} of 0.845 was achieved by the XGB model. The XGB model exhibited the largest drop of 0.061 between the training and testing predictions, meaning that for the testing data, the results were poorer by 6.1% compared to the training data. All the rest of the models result in R^2_{test} being more than 0.87, which means that these models can accurately predict the results in 87% of cases.

Table 8. Models for Tertiary Imbibition Tests

Parameter	ANN	DT	GB	RF	SVM	XGB
$MAPE_{train}$	24.111	21.007	25.340	23.049	12.441	27.192
$RMSE_{train}$	7.432	7.015	7.287	7.108	6.834	54.001
R^2_{train}	0.901	0.912	0.907	0.91	0.914	0.906
AIC_{train}	451.275	438.575	446.953	441.497	432.824	448.791
BIC_{train}	464.778	452.078	460.455	454.999	446.327	462.293
$MAPE_{test,}$	23.398	34.514	26.356	24.254	25.367	20.204
$RMSE_{test}$	7.709	8.184	7.493	7.409	8.204	72.999

Parameter	ANN	DT	GB	RF	SVM	XGB
R^2_{test}	0.889	0.876	0.894	**0.896**	0.889	0.845
AIC_{test}	124.379	127.728	122.787	122.154	127.858	130.132
BIC_{test}	131.041	134.389	129.448	128.815	134.519	136.793

Based on the training metrics, the proposed SVM outperformed the other models. The key difference is in the values of $MAPE_{train}$. $MAPE_{SVM\ train}$ is 12.441, which is 8.566 lower than the second lowest $MAPE_{DT\ train}$. The other metrics also demonstrate the best performance in the training part of the SVM model. However, for the test part, the combination of the metrics does not demonstrate that, and for our case, the testing part is more valuable. There was a marginal difference between the metrics for all the models for the testing part, but all the examining metrics combined suggested that the RF model was the best model for predicting the tertiary imbibition recovery factor. Based on the R2 result, the best performing model was RF with an R^2_{train} of 0.91 and R^2_{test} of 0.896, as shown in Figure 29. The rest of the values of R^2_{train} and R^2_{test} can be seen in Figures 41-45.

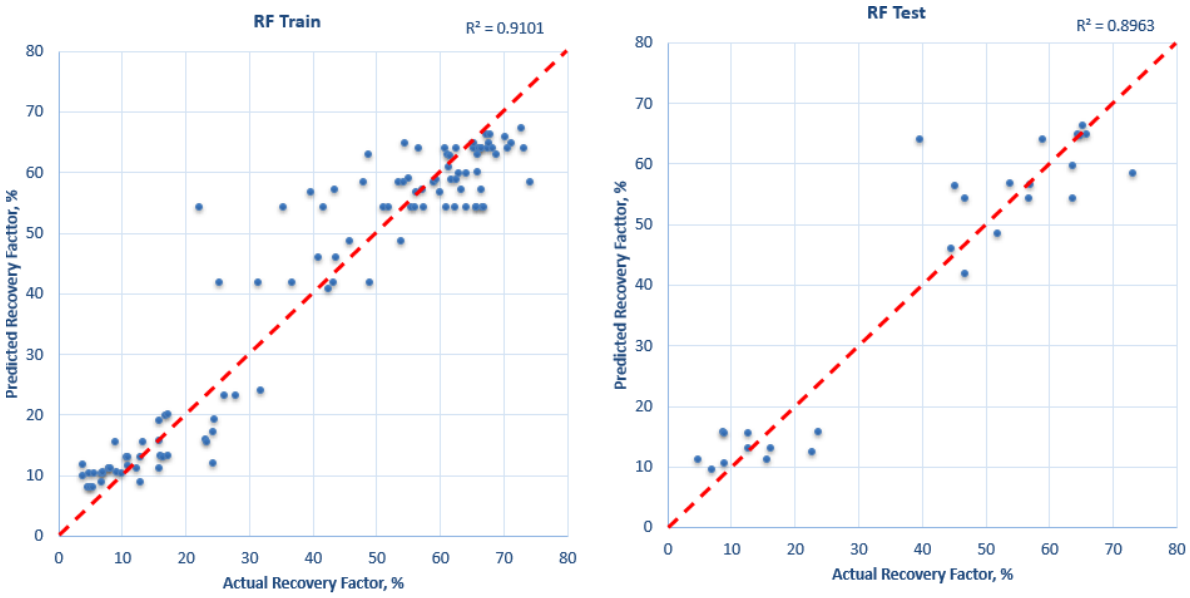

Figure 29. Results of R^2 for RF Model on Tertiary Dataset

GB also demonstrated very similar performance to RF, with R^2_{test} being 0.894. The 0.2% difference between the models indicates that GB can work well with both secondary and tertiary imbibition datasets. However, for the tertiary dataset, RF performed better, and other

supporting metrics proved that. Although the $MAPE_{RF\ test}$ of 24.254 was not the lowest ($MAPE_{XGB\ test}$ = 20.204), the remaining metrics were the lowest: RMSE (7.409), AIC (122.154), and BIC (128.815). These results prove that the RF model is the most effective model for minimizing the percentage error and overfitting.

Almost 90% of the predictions made by the RF model fit the actual data. However, room remains for improvement. As for the secondary dataset, the main source of error was the dataset. If the dataset would be larger consisting not only of 233 data points, out of which 138 data points are left after pre-processing (110 for training and 28 for testing); included information about IFT and contact angle, and contained information about recovery factor in the form of tabular data, the performance of the models could close to 99%. However, despite these limitations, the models can reasonably accurately predict the tertiary imbibition recovery factor.

4.3 Application of Machine Learning Models to Secondary and Tertiary Imbibition

Table 9 summarizes the metrics of the models based on both secondary and tertiary imbibition data. For training, all models achieved $R^2 > 0.85$, and 4 of the models resulted in $R^2 > 0.9$. Thus, there are no issues with the models when training on the data. Even though some models struggled with the training part when the secondary dataset was used (from Table 7, R^2_{train} for DT and SVM are 0.469 and 0.598, respectively), the performance of the models considerably improves when secondary data is combined with the tertiary data. This could be due to the increased amount of data and its diversity. The total number of data points was 395 after cleaning 203 points, of which 162 were for training and 41 were for testing. In addition, the dataset itself becomes more diverse by containing information from both secondary and tertiary data. These improvements help the models run and perform better.

Table 9. Model Results for Secondary and Tertiary Imbibition Tests

Parameter	ANN	DT	GB	RF	SVM	XGB
$MAPE_{train}$	23.481	28.646	17.277	19.955	22.345	33.301
$RMSE_{train}$	7.618	8.440	5.785	6.382	6.320	72.106
R^2_{train}	0.920	0.856	0.930	0.919	0.919	0.888

AIC_{train}	673.893	707.109	584.729	616.567	583.903	709.059
BIC_{train}	698.594	731.810	609.430	641.268	608.198	733.760
$MAPE_{test,}$	27.351	33.457	26.124	31.796	37.150	35.024
$RMSE_{test}$	10.946	10.313	7.546	7.703	10.051	74.943
R^2_{test}	0.885	0.757	**0.895**	0.891	0.816	0.881
AIC_{test}	212.230	207.343	181.73	183.412	196.004	192.986
BIC_{test}	225.939	221.052	195.438	197.121	209.312	206.695

The highest R^2_{train} of 0.93 was achieved by GB, and the lowest R^2_{train} of 0.856 was achieved by DT. According to the supporting metrics, GB achieved the lowest $MAPE_{train}$ of 17.277 and $RMSE_{train}$ of 5.785, and the second lowest in AIC_{train} of 584.729 and BIC_{train} of 609.430.

The highest R^2_{test} of 0.895 is also achieved by GB, and the lowest R^2_{test} of 0.757 is also achieved by DT. Supporting metrics also prove that GB had the lowest MAPE (26.124), RMSE (7.546), AIC (181.73), and BIC (195.438). This proves the previous hypothesis that GB would work well with a dataset containing both secondary and tertiary data. A visual illustration of the predictions made by the GB model compared to the actual data is shown in Figure 30. The rest of the graphs are shown in Figures 46-50.

Given that low-salinity water imbibition mechanisms differ significantly between sandstone and carbonate formations, separate models for each lithology type would likely yield improved accuracy. However, due to the limited size of the dataset for each lithology category, this approach was not feasible in the current study. Future research with a larger and more balanced dataset should explore lithology-specific models to better capture the unique fluid–rock interactions.

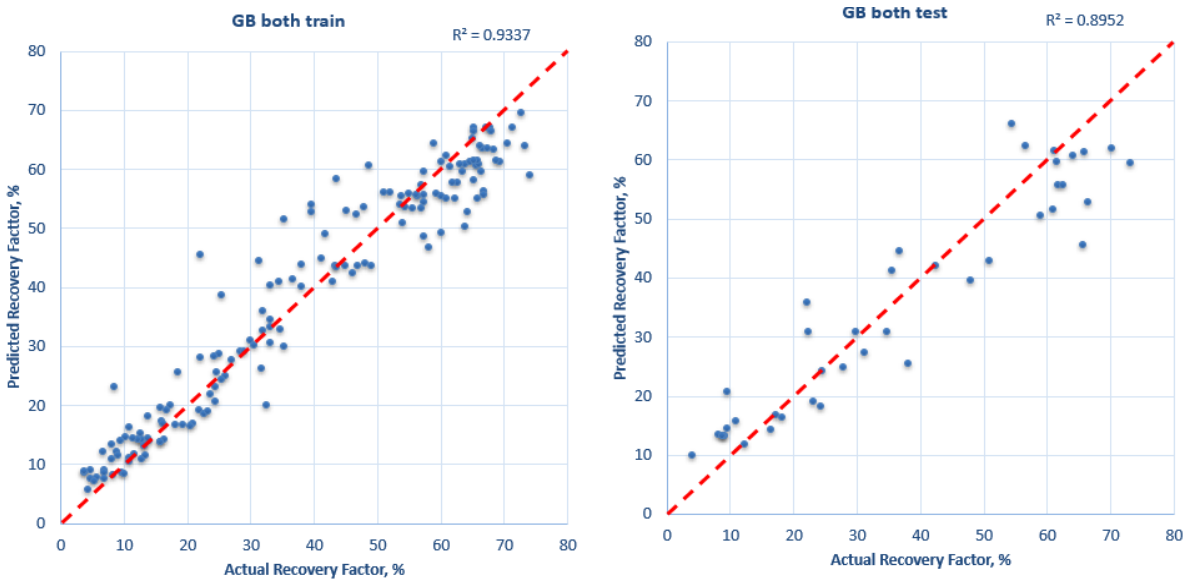

Figure 30. Results of R^2 for the GB Model for Both Secondary and Tertiary Datasets

Analysis across all datasets confirmed that lower salinity levels generally correspond to higher recovery factors, particularly in tertiary imbibition experiments. The correlation coefficient between salinity and recovery factor was negative (–0.45) in the tertiary dataset, affirming that reduced salinity enhances oil recovery. The effect was most prominent in the 500–10,000 ppm range, aligning with known LSWF thresholds. However, beyond ~30,000 ppm, the benefit of salinity reduction appears to plateau or diminish, possibly due to saturation of the wettability alteration mechanism or limited ion exchange.

4.4 Performance of the Best Model

The R^2_{test} of 0.895 indicates that the GB model can properly make predictions in approximately 90% of the time. The R^2_{train} of 0.93 was the highest among all models and datasets, indicating that there is no such combination of data and machine learning model that could result in higher training performance. A drop of 3.5% between training and testing R^2 values could also occur due to the same reasons. Even if the dataset contained 395 data points, almost half of the data is considered as outliers, which did not fall into the 25-75% margin range, leaving only 203 data points to be used for the models to predict without noise. In addition, 89.5% of R^2_{test} is not a limit; this value could be further increased up to 95% and higher if the dataset of IFT and Contact angle were integrated as inputs into the dataset. Human error could be reduced if a larger amount of tabular data with precise readings were used. However, the GB model performs well even with these limitations, and this model can be used for any dataset, either secondary, tertiary, or both.

Figure 31 compares the performance of the GB model on all datasets.

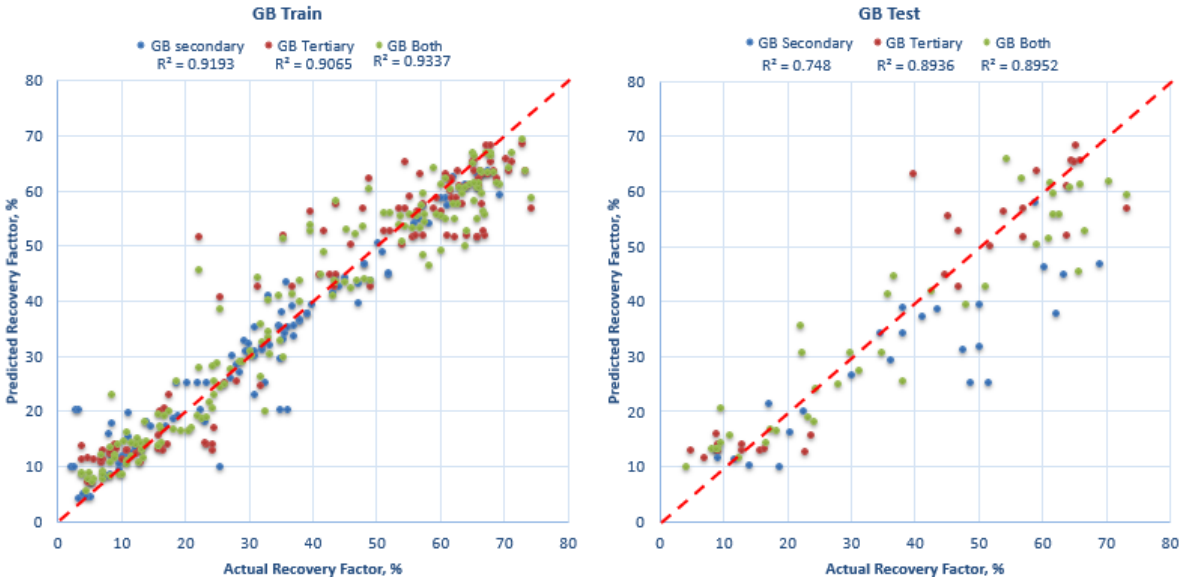

Figure 31. Comparative performance of the GB model

For the training part, the GB model demonstrated high performance, resulting in R^2_{train} being greater than 0.9 for all datasets. For the testing part, the GB model also resulted in high performance; thus, the lowest R^2_{test} value of 0.748 was obtained for the secondary dataset, and for the rest of the datasets, the R^2_{test} is close to 0.9. Although the value of R^2_{test} for secondary imbibition is small compared to the other two, it exhibited the highest performance for the secondary dataset.

A sensitivity analysis of how salinity affects oil recovery was conducted based on the data in Table 10. The only parameter that changes is the salinity, as the core remains the same. Recovery factor values were obtained from Figure 32 (Nasralla et al., 2016)

Table 10. Data from spontaneous imbibition tests (Nasralla et al., 2016)

L (cm)	*D (cm)*	Φ (%)	*Swi (%)*	Lithology	Salinity (ppm)	T (°C)	RF (%)
5.01	3.8	20.8	12	Carbonate	239400	70	5.4
5.01	3.8	20.8	12	Carbonate	43700	70	10.0
5.01	3.8	20.8	12	Carbonate	8740	70	12.3

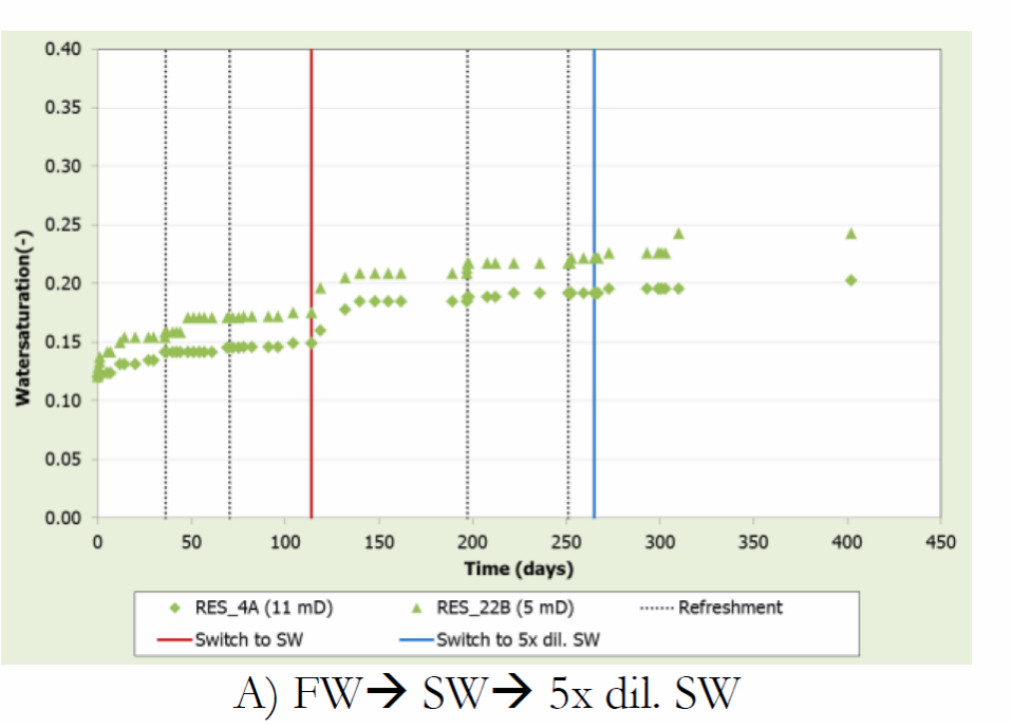

Figure 32. Spontaneous Imbibition Curve Using Water with Different Salinities (Nasralla et al., 2016)

The predictions of the GB model based on these data are shown in Figure 33 The blue and red columns represent actual and predicted RF values, respectively. The difference between the actual and predicted values is clearly shown. The model performed better as the salinity of the water decreased. The highest deviation was obtained at the highest salinity. This occurs because the goal of the model is not to predict the RF of high-salinity water, and the value of 239400 ppm salinity is an outlier. However, even with this deviation, the trend in the RF values can be observed. As the salinity decreases from 239400 to 8740 ppm, the model predicts that oil recovery will increase from 8.5 to 12.6. The lower the water salinity, the better the GB model can predict the results.

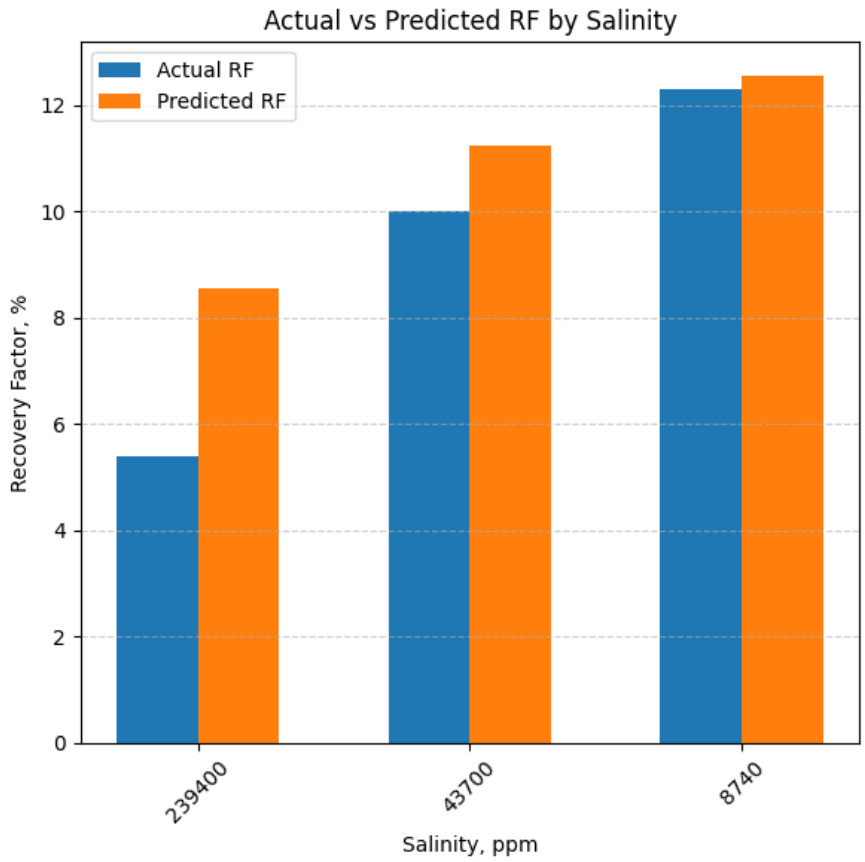

Figure 33. Comparison of Actual and Predicted Values of the GB Model

The performance of the GB model for Carbonate rock is shown in Figure 34. As it can be seen, the experimental and predicted values for the temperature of 70 °C differ by 0.5-4% of recovery factor for all of the salinity values. Predictions values for lower temperature of 50 °C are lower by roughly 2-4% of recovery factor. The model performance aligns with the theory behind it: the lower the salinity becomes the higher the oil recovery for carbonate rock.

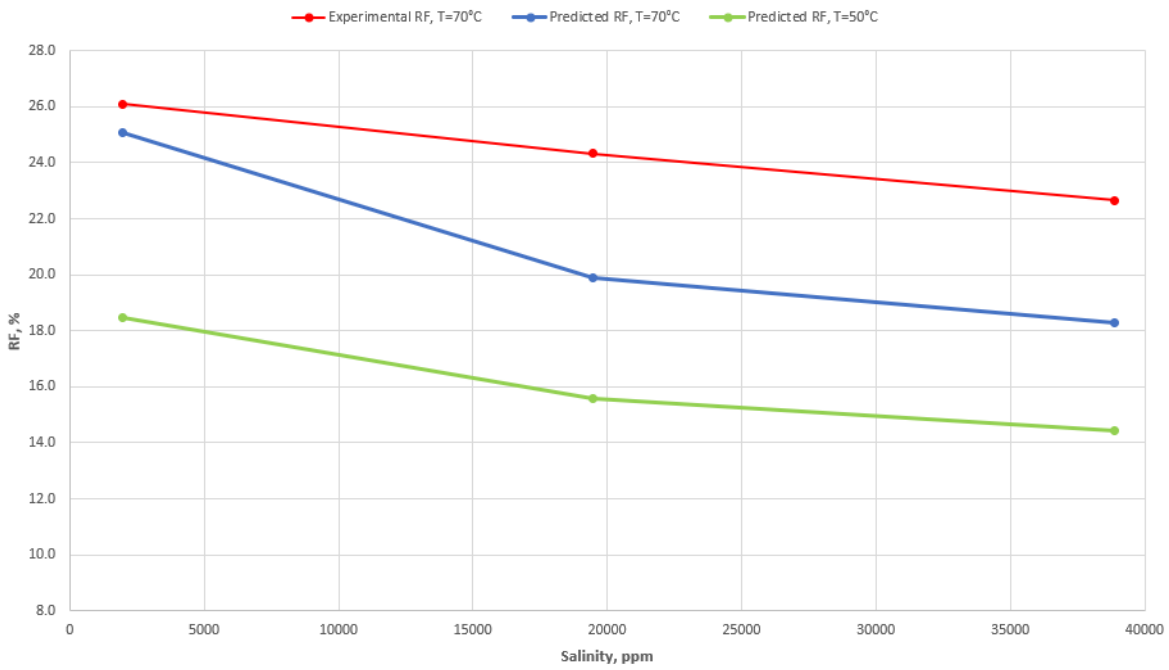

Figure 34. Performance of the GB model for Carbonate Core

The same trend is obtained during analysis of the performance of the GB model for the sandstone core shown in Figure 35. Experimental and predicted values for temperature of 60 °C differ by less than 1% of oil recovery for all of the salinities. Predictions for lower temperature of 40 °C show lower oil recoveries by 2-5% for the same salinity levels. The trend for the lower temperature is the same as for the carbonate rock: the lower the temperature the less the oil recovery during spontaneous imbibition test.

GB model predicts more accurate results for sandstone cores rather than for carbonate cores. It can be justified by the fact that there is more data in this range of temperature and salinities combined for the sandstone than carbonate rock.

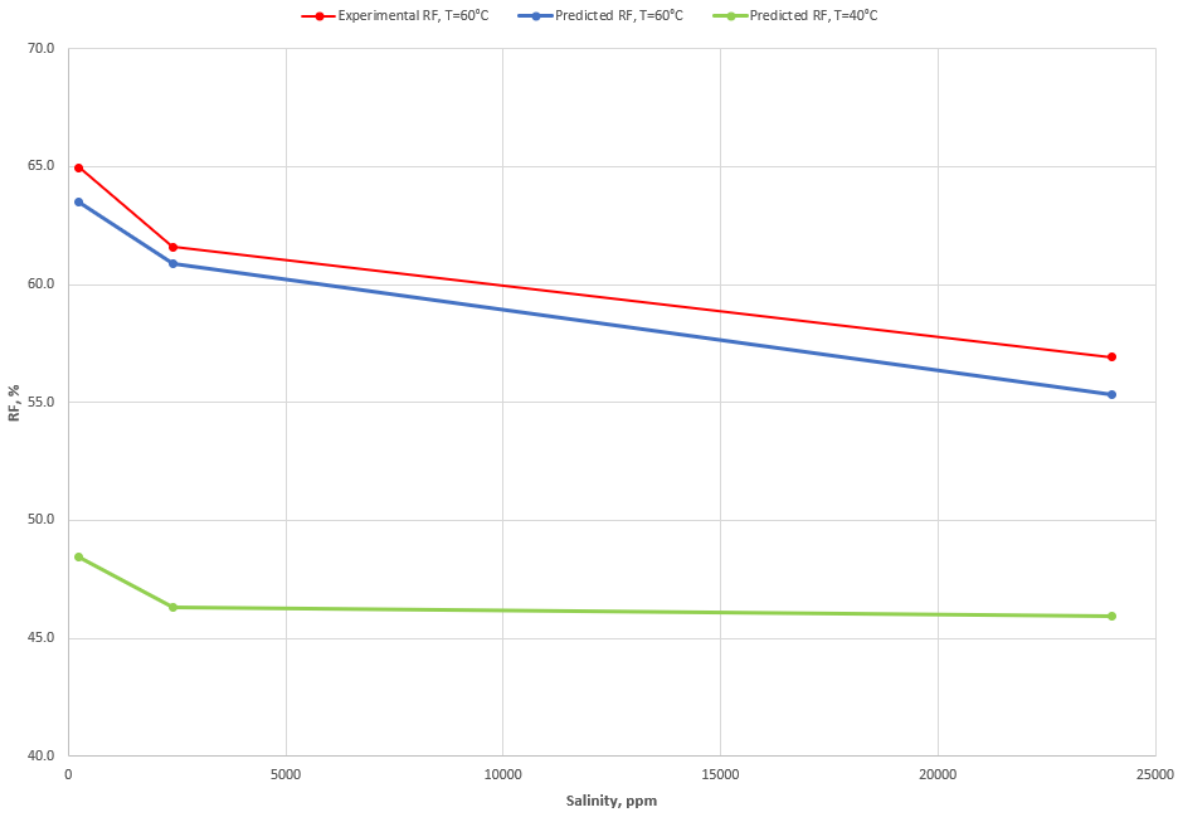

Figure 35. Performance of the GB model for Sandstone Core

Chapter 5: Conclusion and Recommendations

The study explored the usability of machine learning models in predicting recovery factors in secondary and tertiary spontaneous imbibition experiments. To do so, data from 25 research papers were gathered, including input parameters such as the length of the core, diameter of the core, porosity of the core, lithology, initial water saturation, salinity of the brine, temperature of the experiment, and output as absolute oil recovery. Data from 395 spontaneous imbibition experiments were collected, and six machine learning models were trained and tested.

For the secondary dataset a maximum value of R^2_{test} of 0.748 was achieved by GB. For the tertiary dataset GB performed in R^2_{test} being 0.896 and for the combined dataset R^2_{test} of 0.895 was achieved. After thorough analysis, it was found that the Gradient Boosting machine learning model exhibited superior performance compared to other models based on secondary and combined datasets, and for the tertiary RF model outperformed GB by 0.2%. Combining all of that, GB model is selected to be the best performing model for spontaneous imbibition absolute oil recovery prediction.

Most of the models performed well with tertiary and combined datasets. The prediction accuracy close to 90% was achieved by several machine learning models. However, the performance of the models can be further improved and this was caused by the limitations of the datasets during the data gathering part. These limitations strongly affect the secondary predictions, where 75% accuracy was achieved.

The future work should focus on mitigating the factors, which affect the accuracy of the models and resulting in the prediction accuracy being more than 90%. One of the ways is to expand the datasets by adding more data of both secondary and tertiary spontaneous imbibition data. Expanding the number of the tests is not the only way to make more accurate predictions. Addition of different input parameters such as interfacial tension and contact angle of the system before the test should increase the accuracy of the machine learning models. Also, it is better to find the data in a tabular form rather than extracting the output values of the recovery factor manually using the Plot Digitizer tool. This could help reduce

the human error caused by manual extraction of the data from the graphs of spontaneous imbibition experiments.

Overall, all of the models were implemented and tested with different datasets. The main goal of the research was achieved, and future research can be further done to investigate the best-performing machine learning models.

References

Alfarge, D., Wei, M. and Bai, B. (2020). Chemical enhanced oil recovery methods for unconventional reservoirs. *In Developments in Petroleum Science*, 67, pp. 141-163. Elsevier. doi: https://doi.org/10.1016/B978-0-12-818343-4.00007-3

Al-Harrasi, A. S., Al-Maamari, R. S., & Masalmeh, S. (2012, November). Laboratory investigation of low salinity waterflooding for carbonate reservoirs. In Abu Dhabi International Petroleum Exhibition and Conference (pp. SPE-161468). SPE.

Austad, T., & Standnes, D. C. (2003). Spontaneous imbibition of water into oil-wet carbonates. Journal of Petroleum Science and Engineering, 39(3–4), 363–376. https://doi.org/10.1016/S0920-4105(03)00075-5

Austad, T., Rezaeidoust, A., & Puntervold, T. (2010). Chemical mechanisms of low salinity water flooding in sandstone reservoirs. *SPE Improved Oil Recovery Symposium*. https://doi.org/10.2118/129767-MS

Anderson, W. G. (1986). Wettability literature survey—Part 1: Rock/oil/brine interactions and the effects of core handling on wettability. Journal of Petroleum Technology, 38(10), 1125–1144. https://doi.org/10.2118/13932-PA

Behbahani, H. S., Di Donato, G., & Blunt, M. J. (2006). Simulation of counter-current imbibition in water-wet fractured reservoirs. Journal of Petroleum Science and Engineering, 50(1–2), 21–39.https://doi.org/10.1016/j.petrol.2005.09.001

Bishop, C. M. (1995). Neural networks for pattern recognition. Oxford university press.

Breiman, L. (1996). Bagging predictors. Machine learning, 24, 123-140.

Breiman, L. (2001). Random forests. Machine learning, 45, 5-32.

Buckley, J. S., Liu, Y., & Monsterleet, S. (1998). Mechanisms of wetting alteration by crude oils. SPE Journal, 3(1), 54–61. https://doi.org/10.2118/37230-PA

Cao, J., Chen, Y., Wang, X., Zhang, J., Li, Y., Hua, Z., ... & Zhao, S. (2022). Low-salinity nanofluid–A smart fluid enhanced oil recovery method. Colloids and Surfaces A: Physicochemical and Engineering Aspects, 648, 129204.

Chen, T., & Guestrin, C. (2016, August). Xgboost: A scalable tree boosting system. In Proceedings of the 22nd acm sigkdd international conference on knowledge discovery and data mining (pp. 785-794).

Chen, W., & Schechter, D. S. (2021). Surfactant selection for enhanced oil recovery based on surfactant molecular structure in unconventional liquid reservoirs. Journal of Petroleum Science and Engineering, 196, 107702.

Cil, M. B., Al-Saidi, M., & Blunt, M. J. (1998). A study of spontaneous imbibition using numerical simulation. Journal of Petroleum Science and Engineering, 20(3–4), 213–226. https://doi.org/10.1016/S0920-4105(98)00018-0

Cristianini, N., & Shawe-Taylor, J. (2000). An introduction to support vector machines and other kernel-based learning methods. Cambridge university press.

De Myttenaere, A., Golden, B., Le Grand, B., & Rossi, F. (2016). Mean absolute percentage error for regression models. Neurocomputing, 192, 38-48.

Denney, D. (2012). Eor potential in the Middle East: Current and future trends. *OnePetro*. doi: https://doi.org/10.2118/0112-0070-JPT

Faska, Z., Khrissi, L., Haddouch, K., & El Akkad, N. (2023). A robust and consistent stack generalized ensemble-learning framework for image segmentation. Journal of Engineering and Applied Science, 70(1), 74.

Fathi, S. J., Austad, T., & Strand, S. (2010). “Smart water” as a wettability modifier in chalk: the effect of salinity and ionic composition. Energy & fuels, 24(4), 2514-2519.

Fathi, S. J., Austad, T., & Strand, S. (2011). Water-based enhanced oil recovery (EOR) by “smart water”: Optimal ionic composition for EOR in carbonates. Energy & fuels, 25(11), 5173-5179.

Fathi, S. J., Austad, T., & Strand, S. (2011). Effect of water-extractable carboxylic acids in crude oil on wettability in carbonates. Energy & fuels, 25(6), 2587-2592.

Fathi, S. J., Austad, T., Strand, S., & Puntervold, T. (2010). Wettability alteration in carbonates: The effect of water-soluble carboxylic acids in crude oil. Energy & Fuels, 24(5), 2974-2979.

Feldmann, F., Strobel, G. J., Masalmeh, S. K., & AlSumaiti, A. M. (2020). An experimental and numerical study of low salinity effects on the oil recovery of carbonate rocks combining spontaneous imbibition, centrifuge method and coreflooding experiments. Journal of Petroleum Science and Engineering, 190, 107045.

Firoozabadi, A. (2000). Recovery mechanisms in fractured reservoirs and field performance. Journal of Canadian Petroleum Technology, 39(11).

Friedman, J. H. (2001). Greedy function approximation: a gradient boosting machine. Annals of statistics, 1189-1232.

Gachuz-Muro, H., & Sohrabi, M. (2014, September). Smart water injection for heavy oil recovery from naturally fractured reservoirs. In SPE Latin America and Caribbean Heavy and Extra Heavy Oil Conference (p. D021S012R002). SPE.

Ghandi, E., Parsaei, R., & Riazi, M. (2019). Enhancing the spontaneous imbibition rate of water in oil-wet dolomite rocks through boosting a wettability alteration process using carbonated smart brines. Petroleum Science, 16, 1361-1373.

Goodfellow, I., Bengio, Y., Courville, A., & Bengio, Y. (2016). Deep learning (Vol. 1, No. 2). Cambridge: MIT press.

Guo, J., Li, M., Chen, C., Tao, L., Liu, Z., & Zhou, D. (2020). Experimental investigation of spontaneous imbibition in tight sandstone reservoirs. *Journal of Petroleum Science and Engineering*, *193*, 107395.

Harimi, B., Masihi, M., Mirzaei-Paiaman, A., & Hamidpour, E. (2019). Experimental study of dynamic imbibition during water flooding of naturally fractured reservoirs. Journal of Petroleum Science and Engineering, 174, 1-13.

Hidayat, F., Erfando, T., & Maulana, B. F. (2018). Spontaneous imbibition test of low salinity injection at low saline waxy crude carbonate. Journal of Earth Energy Engineering, 7(2), 14-22.

Hincapie, R. E., Borovina, A., Neubauer, E., Tahir, M., Saleh, S., Arekhov, V., Biernat, M., & Clemens, T. (2022). Recovery Observations from Alkali, Nanoparticles and Polymer Flooding as Combined Processes. Polymers, 14(3), 603. https://doi.org/10.3390/polym14030603

Karimi, M., Al-Maamari, R. S., Ayatollahi, S., & Mehranbod, N. (2016). Wettability alteration and oil recovery by spontaneous imbibition of low salinity brine into

carbonates: Impact of Mg2+, SO42− and cationic surfactant. Journal of Petroleum Science and Engineering, 147, 560-569.

Karnanda, W., Benzagouta, M. S., AlQuraishi, A., & Amro, M. M. (2013). Effect of temperature, pressure, salinity, and surfactant concentration on IFT for surfactant flooding optimization. Arabian Journal of Geosciences, 6, 3535-3544.Katende, A., & Sagala, F. (2019). A critical review of low salinity water flooding: Mechanism, laboratory and field application. Journal of Molecular Liquids, 278, 627-649.

Kathel, P., & Mohanty, K. (2018). Dynamic surfactant-aided imbibition in fractured oil-wet carbonates. Journal of Petroleum Science and Engineering. https://doi.org/10.1016/J.PETROL.2018.06.088.

Kazemi, H., Merrill Jr, L. S., Porterfield, K. L., & Zeman, P. R. (1976). Numerical simulation of water-oil flow in naturally fractured reservoirs. Society of Petroleum Engineers Journal, 16(6), 317–326.https://doi.org/10.2118/5719-PA

Khan, M. Y., Qayoom, A., Nizami, M. S., Siddiqui, M. S., Wasi, S., & Raazi, S. M. K. U. R. (2021). Automated Prediction of Good Dictionary EXamples (GDEX): A Comprehensive Experiment with Distant Supervision, Machine Learning, and Word Embedding-Based Deep Learning Techniques. Complexity, 2021(1), 2553199.

Kharrat, R.; Zallaghi, M.; Ott, H. (2021) Performance Quantification of Enhanced Oil Recovery Methods in Fractured Reservoirs. Energies 2021, 14, 4739x

Khoramian, R., Kharrat, R., Pourafshary, P., Golshokooh, S., & Hashemi, F. (2022). Spontaneous imbibition oil recovery by natural surfactant/nanofluid: An experimental and theoretical study. Nanomaterials, 12(20), 3563.

Komarasamy, G., & Ravishankar, T. N. (2022). The Application of Decision Tree Method for Data Mining. Technoarete Transactions on Intelligent Data Mining and Knowledge Discovery, 2(3).

Kvålseth, T. O. (2017). On normalized mutual information: measure derivations and properties. Entropy, 19(11), 631.

Liu, X., Yan, L., Gao, Q., Liu, Y., Huang, H., & Liu, S. (2022). Effect of Salinity on the Imbibition Recovery Process of Tight Sandstone Reservoirs. Processes, 10(2), 228.

Loh, W. Y. (2011). Classification and regression trees. Wiley interdisciplinary reviews: data mining and knowledge discovery, 1(1), 14-23.

Lu, J., Goudarzi, A., Chen, P., Kim, D. H., Delshad, M., Mohanty, K. K., ... & Pope, G. A. (2014). Enhanced oil recovery from high-temperature, high-salinity naturally fractured carbonate reservoirs by surfactant flood. Journal of Petroleum Science and Engineering, 124, 122-131.

Ma, S., Morrow, N. R., & Zhang, X. (1997). Generalized scaling of spontaneous imbibition data for strongly water-wet systems. *Journal of Petroleum Science and Engineering*, *18*(3–4), 165–178. https://doi.org/10.1016/S0920-4105(97)00022-

Mahani, H., Keya, A. L., Berg, S., Bartels, W. B., Nasralla, R., & Rossen, W. R. (2015). Insights into the mechanism of wettability alteration by low-salinity flooding (LSF) in carbonates. Energy & Fuels, 29(3), 1352-1367.

Mahmoudzadeh, A., Fatemi, M., & Masihi, M. (2022). Microfluidics experimental investigation of the mechanisms of enhanced oil recovery by low salinity water flooding in fractured porous media. Fuel, 314, 123067.

Mahzari, P., Sohrabi, M., & Façanha, J. M. (2019). The decisive role of microdispersion formation in improved oil recovery by low-salinity-water injection in sandstone formations. SPE Journal, 24(06), 2859-2873.

Maricic, V.K., Lekovic, B. and Danilović, D. (2014). Factors influencing successful implementation of enhanced oil recovery projects. doi: 10.5937/podrad1425041K

Mason, G., & Morrow, N. R. (1994). Effect of contact angle on capillary displacement curvatures in pore throats formed by spheres. Journal of Colloid and Interface Science, 168(1), 130–141.https://doi.org/10.1006/jcis.1994.1402

Mehraban, M. F., Rostami, P., Afzali, S., Ahmadi, Z., Sharifi, M., & Ayatollahi, S. (2020). Brine composition effect on the oil recovery in carbonate oil reservoirs: A comprehensive experimental and CFD simulation study. Journal of Petroleum Science and Engineering, 191, 107149.

Mohammadi, S., Kord, S., & Moghadasi, J. (2019). An experimental investigation into the spontaneous imbibition of surfactant assisted low salinity water in carbonate rocks. Fuel, 243, 142-154.

Morrow, N. R. (1990). Wettability and its effect on oil recovery. Journal of Petroleum Technology, 42(12), 1476–1484. https://doi.org/10.2118/21621-PA

Morrow, N. R., & Mason, G. (2001). Recovery of oil by spontaneous imbibition. *Current Opinion in Colloid & Interface Science*, *6*(4), 321–337. https://doi.org/10.1016/S1359-0294(01)00100-5

Muriel, H. et al. (2020). Technical and economical screening of chemical EOR methods for the offshore. *OnePetro*. doi: https://doi.org/10.4043/30740-MS

Nasralla, R. A., van der Linde, H. A., Marcelis, F. H., Mahani, H., Masalmeh, S. K., Sergienko, E., ... & Basu, S. (2016, November). Low salinity waterflooding for a carbonate reservoir experimental evaluation and numerical interpretation. In Abu Dhabi International Petroleum Exhibition and Conference (p. D011S005R003). SPE.

Neath, A. A., & Cavanaugh, J. E. (2012). The Bayesian information criterion: background, derivation, and applications. Wiley Interdisciplinary Reviews: Computational Statistics, 4(2), 199-203.

Nolan, D.P. (2010). Overview of oil and Gas Facilities, Handbook of Fire and Explosion Protection Engineering Principles (Second Edition). William Andrew Publishing. doi: https://doi.org/10.1016/B978-1-4377-7857-1.00002-1.

Nowrouzi, I., Manshad, A. K., & Mohammadi, A. H. (2019). Effects of ions and dissolved carbon dioxide in brine on wettability alteration, contact angle and oil production in smart water and carbonated smart water injection processes in carbonate oil reservoirs. Fuel, 235, 1039-1051.

Nowrouzi, I., Mohammadi, A. H., & Manshad, A. K. (2020). Water-oil interfacial tension (IFT) reduction and wettability alteration in surfactant flooding process using extracted saponin from Anabasis Setifera plant. Journal of Petroleum Science and Engineering, 189, 106901.

Qisheng, M. and Yongchun, T. (2023). Molecular designs of Enhanced Oil Recovery Chemicals, Recovery Improvement. Gulf Professional Publishing. doi: https://doi.org/10.1016/B978-0-12-823363-4.00006-6

Patel, H. S., & Meher, R. (2018). Simulation of counter-current imbibition phenomenon in a double phase flow through fracture porous medium with capillary pressure. *Ain Shams Engineering Journal*, *9*(4), 2163-2169.

Puntervold, T., Strand, S., & Austad, T. (2009). Coinjection of seawater and produced water to improve oil recovery from fractured North Sea chalk oil reservoirs. Energy & fuels, 23(5), 2527-2536.

Ragab, A. and Mansour, E.M. (2021). Enhanced oil recovery: chemical flooding. *Geophysics and Ocean Waves Studies*, 51. doi: 10.5772/intechopen.90335

Ravari, R. R. (2011). Water-based eor in limestone by smart water: a study of surface chemistry.

Romanuka, J., Hofman, J. P., Ligthelm, D. J., Suijkerbuijk, B. M., Marcelis, A. H., Oedai, S., ... & Austad, T. (2012, April). Low salinity EOR in carbonates. In SPE Improved Oil Recovery Conference? (pp. SPE-153869). SPE.

Roostaei, A. (2014). Enhanced oil recovery (EOR) by" smart water" in carbonates reservoir (Master's thesis, University of Stavanger, Norway).

Rumelhart, D. E., Hinton, G. E., & Williams, R. J. (1986). Learning representations by back-propagating errors. nature, 323(6088), 533-536.

Saleh, S., Neubauer, E., Borovina, A., Hincapie, R. E., Clemens, T., & Ness, D. (2021). Wettability changes due to nanomaterials and alkali—A proposed formulation for EOR. Nanomaterials, 11(9), 2351.

Sahraei, A., Chamorro, A., Kraft, P., & Breuer, L. (2021). Application of machine learning models to predict maximum event water fractions in streamflow. Frontiers in Water, 3, 652100.

Sarsenbekuly, B., Aidarova, S., & Ibrashev, K. (2020). Imbibition enhancing oil recovery mechanism of the two surfactants. Physics of Fluids, 32, 047103. https://doi.org/10.1063/5.0005106.

Schechter, D. S., Zhou, D., & Orr Jr, F. M. (1991). Low IFT drainage and imbibition. Journal of Petroleum Science and Engineering, 6(4), 283–300.

Schumi, B., Clemens, T., Wegner, J., Ganzer, L., Kaiser, A., Hincapie, R. E., & Leitenmüller, V. (2019, June). Alkali Co-Solvent Polymer Flooding of High TAN Number Oil: Using Phase Experiments, Micro-Models and Corefloods for Injection Agent Selection. In SPE Europec featured at EAGE Conference and Exhibition (p. D041S010R001). SPE.

Sepehri, M., Moradi, B., Emamzadeh, A., & Mohammadi, A. H. (2019). Experimental study and numerical modeling for enhancing oil recovery from carbonate reservoirs by nanoparticle flooding. Oil & Gas Science and Technology–Revue d'IFP Energies nouvelles, 74, 5.

Shariatpanahi, S. F., Strand, S., & Austad, T. (2010). Evaluation of water-based enhanced oil recovery (EOR) by wettability alteration in a low-permeable fractured limestone oil reservoir. Energy & Fuels, 24(11), 5997-6008.

Shehata, A. M., & Nasr-El-Din, H. A. (2017). Laboratory investigations to determine the effect of connate-water composition on low-salinity waterflooding in sandstone reservoirs. SPE Reservoir Evaluation & Engineering, 20(01), 059-076.

Sheng, J. J. (2014). Critical review of low-salinity waterflooding. *Journal of Petroleum Science and Engineering*, *120*, 216–224. https://doi.org/10.1016/j.petrol.2014.05.026

Smithson, T. (2016). Defining Reservoir Drive Mechanisms. *Schlumberger*.

Smola, A. J., & Schölkopf, B. (2004). A tutorial on support vector regression. Statistics and computing, 14, 199-222.

Sohrabi, M., Mahzari, P., Farzaneh, S. A., Mills, J. R., Tsolis, P., & Ireland, S. (2017). Novel insights into mechanisms of oil recovery by use of low-salinity-water injection. Spe Journal, 22(02), 407-416.

Somasundaran, P., & Zhang, L. (2006). Adsorption of surfactants on minerals for wettability control in improved oil recovery processes. Journal of petroleum science and engineering, 52(1-4), 198-212.

Song, J., Wang, Q., Shaik, I., Puerto, M., Bikkina, P., Aichele, C., ... & Hirasaki, G. J. (2020). Effect of salinity, Mg2+ and SO42− on "smart water"-induced carbonate wettability

alteration in a model oil system. Journal of colloid and interface science, 563, 145-155.

Sorop, T. G., Masalmeh, S. K., Suijkerbuijk, B. M., van der Linde, H. A., Mahani, H., Brussee, N. J., ... & Coorn, A. B. (2015, November). Relative permeability measurements to quantify the low salinity flooding effect at field scale. In Abu Dhabi International Petroleum Exhibition and Conference (p. D021S024R003). SPE.

Standnes, D. C., & Austad, T. (2000). Wettability alteration in chalk: Preparation of core material and oil properties. *Journal of Petroleum Science and Engineering*, *28*(3), 111–121. https://doi.org/10.1016/S0920-4105(00)00083-8

Strand, S., Puntervold, T., & Austad, T. (2008). Effect of temperature on enhanced oil recovery from mixed-wet chalk cores by spontaneous imbibition and forced displacement using seawater. Energy & Fuels, 22(5), 3222-3225.

Sukee, A., Nunta, T., Fongkham, N., Yoosook, H., Jeennakorn, M., Harbottle, D., ... & Tangparitkul, S. (2022). Effects of brine valency and concentration on oil displacement by spontaneous imbibition: An interplay between wettability alteration and reduction in the oil-brine interfacial tension. Journal of Molecular Liquids, 365, 120089.

Suykens, J. A., & Vandewalle, J. (1999). Least squares support vector machine classifiers. Neural processing letters, 9, 293-300.

Tang, G. Q., & Morrow, N. R. (1999). Influence of brine composition and fines migration on crude oil/brine/rock interactions and oil recovery. *Journal of Petroleum Science and Engineering*, *24*(2–4), 99–111. https://doi.org/10.1016/S0920-4105(99)00034-0

Tavassoli, Z., Zimmerman, R. W., & Blunt, M. J. (2005). Analysis of counter-current imbibition with gravity in weakly water-wet systems. Journal of Petroleum Science and Engineering, 48(1–2), 94–104.https://doi.org/10.1016/j.petrol.2005.05.005

Tetteh, J., Janjang, N. M., & Barati, R. (2018, April). Wettability alteration and enhanced oil recovery using low salinity waterflooding in limestone rocks: A mechanistic study. In

SPE Kingdom of Saudi Arabia Annual Technical Symposium and Exhibition (pp. SPE-192425). SPE.

Tian, W., Wu, K., Gao, Y., Chen, Z., Gao, Y., & Li, J. (2021). A critical review of enhanced oil recovery by imbibition: Theory and practice. Energy & Fuels, 35(7), 5643-5670.

Suijkerbuijk, B. M., Hofman, J. P., Ligthelm, D. J., Romanuka, J., Brussee, N., van derLinde, H. A., & Marcelis, A. H. (2012, April). Fundamental investigations into wettability and low salinity flooding by parameter isolation. In the SPE Improved Oil Recovery Conference? (pp. SPE-154204). SPE.

Vapnik, V. (2000). The nature of statistical learning theory. SpringerVerlag New York. Inc., New York, NY, USA.

Vijapurapu, C. S., & Rao, D. N. (2004). Compositional effects of fluids on spreading, adhesion and wettability in porous media. Colloids and Surfaces A: Physicochemical and Engineering Aspects, 241(1-3), 335-342.

Vilhena, O., Farzaneh, A., Pola, J., March, R., Sisson, A., & Sohrabi, M. (2020). New insights into spontaneous imbibition processes in unfractured and fractured carbonate cores with stress-induced apertures. *SPE Reservoir Evaluation & Engineering*, *23*(02), 722-740.

Vrieze, S. I. (2012). Model selection and psychological theory: a discussion of the differences between the Akaike information criterion (AIC) and the Bayesian information criterion (BIC). Psychological methods, 17(2), 228.

Wang, H., & Xu, D. (2017). Parameter selection method for support vector regression based on adaptive fusion of the mixed kernel function. Journal of Control Science and Engineering, 2017(1), 3614790.

Willmott, C. J., & Matsuura, K. (2005). Advantages of the mean absolute error (MAE) over the root mean square error (RMSE) in assessing average model performance. Climate research, 30(1), 79-82.

Yang, J., Dong, Z., Dong, M., Yang, Z., Lin, M., Zhang, J., & Chen, C. (2016). Wettability alteration during low-salinity waterflooding and the relevance of divalent ions in this process. Energy & Fuels, 30(1), 72-79.

Zaeri, M. R., Hashemi, R., Shahverdi, H., & Sadeghi, M. (2018). Enhanced oil recovery from carbonate reservoirs by spontaneous imbibition of low salinity water. Petroleum Science, 15, 564-576.

Zaeri, M. R., Shahverdi, H., Hashemi, R., & Mohammadi, M. (2019). Impact of water saturation and cation concentrations on wettability alteration and oil recovery of carbonate rocks using low-salinity water. Journal of Petroleum Exploration and Production Technology, 9, 1185-1196.

Zhang, T., Lin, W., Vogelmann, A. M., Zhang, M., Xie, S., Qin, Y., & Golaz, J. C. (2021). Improving convection trigger functions in deep convective parameterization schemes using machine learning. Journal of Advances in Modeling Earth Systems, 13(5), e2020MS002365.

Zhang, P., Tweheyo, M. T., & Austad, T. (2006). Wettability alteration and improved oil recovery in chalk: The effect of calcium in the presence of sulfate. Energy & fuels, 20(5), 2056-2062.

Zhang, L., Zhang, J., Wang, Y., Yang, R., Zhang, Y., Gu, J., ... & Ren, S. (2018). Experimental investigation of low-salinity water flooding in a low-permeability oil reservoir. Energy & Fuels, 32(3), 3108-3118.

Zhao, M., Cheng, Y., Wu, Y., Dai, C., Gao, M., Yan, R., & Guo, X. (2022). Enhanced oil recovery mechanism by surfactant-silica nanoparticles imbibition in ultra-low permeability reservoirs. Journal of Molecular Liquids, 348, 118010.

Zhou, D., Jia, L., Kamath, J., & Kovscek, A. R. (2002). Scaling of counter-current imbibition processes in low-permeability porous media. *Journal of Petroleum Science and Engineering*, *33*(1–3), 61–74. https://doi.org/10.1016/S0920-4105(01)00176-0

Zhou, H., Zhang, Q., Dai, C., Li, Y., Lv, W., Wu, Y., ... & Zhao, M. (2019). Experimental investigation of spontaneous imbibition process of nanofluid in ultralow permeable reservoir with nuclear magnetic resonance. Chemical Engineering Science, 201, 212-221.

Appendix

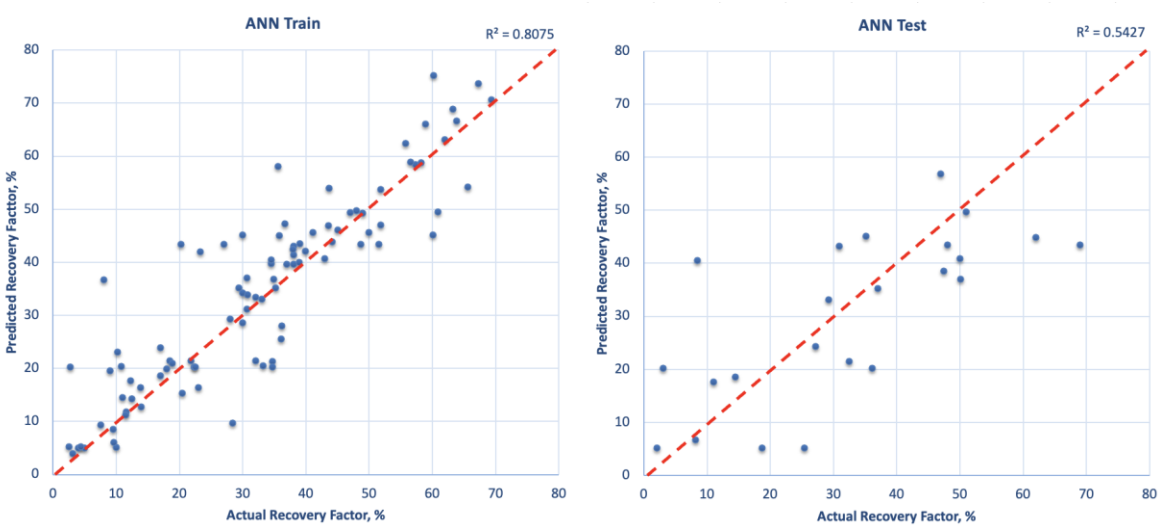

Figure 36. Results of R^2 for the ANN Model for the Secondary Dataset

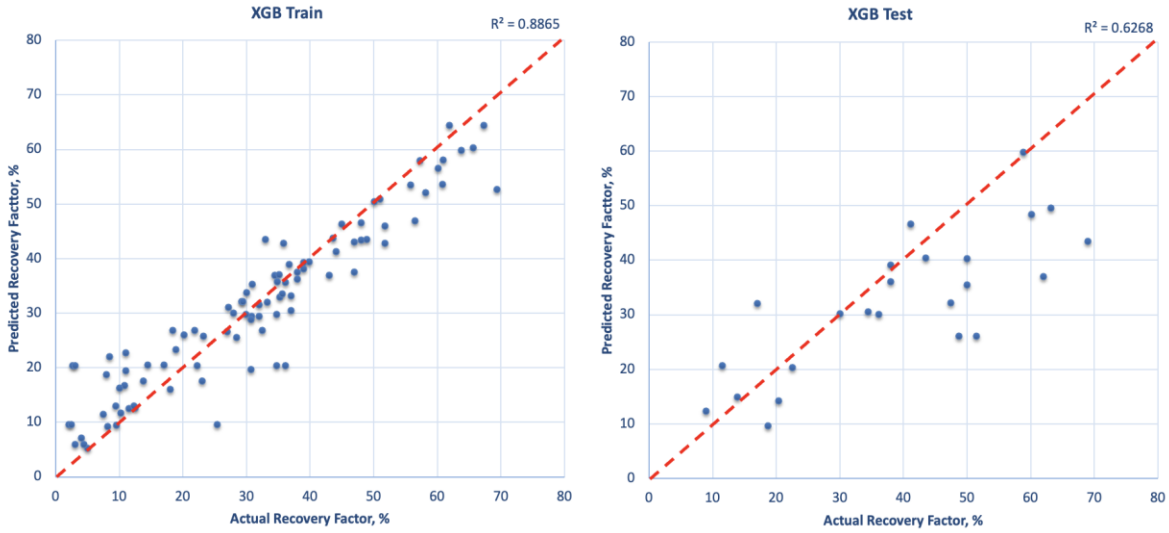

Figure 37. Results of R^2 for the XGB Model for the Secondary Dataset

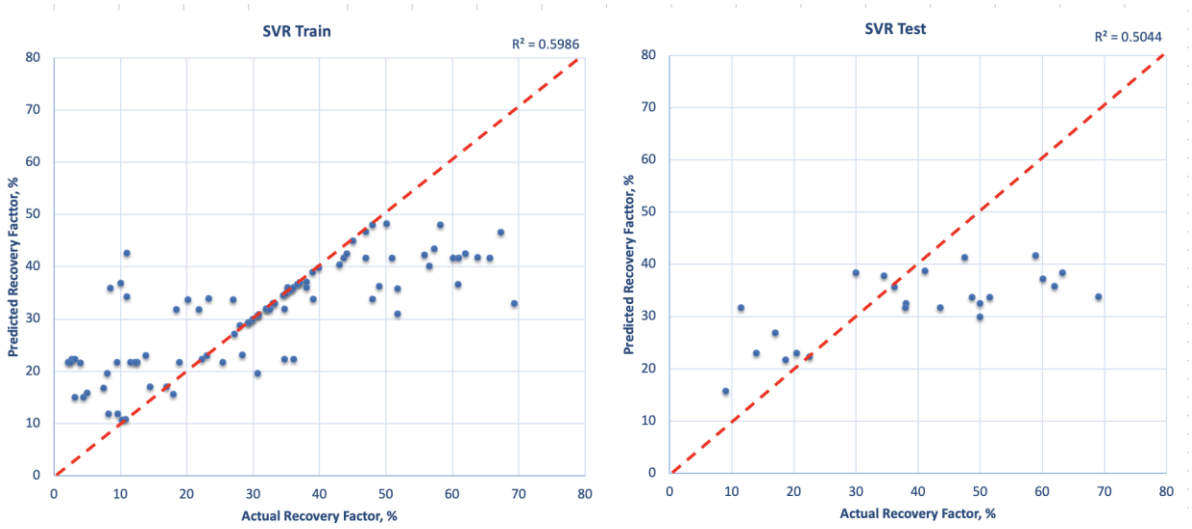

Figure 38. Results of R^2 for the SVR Model for the Secondary Dataset

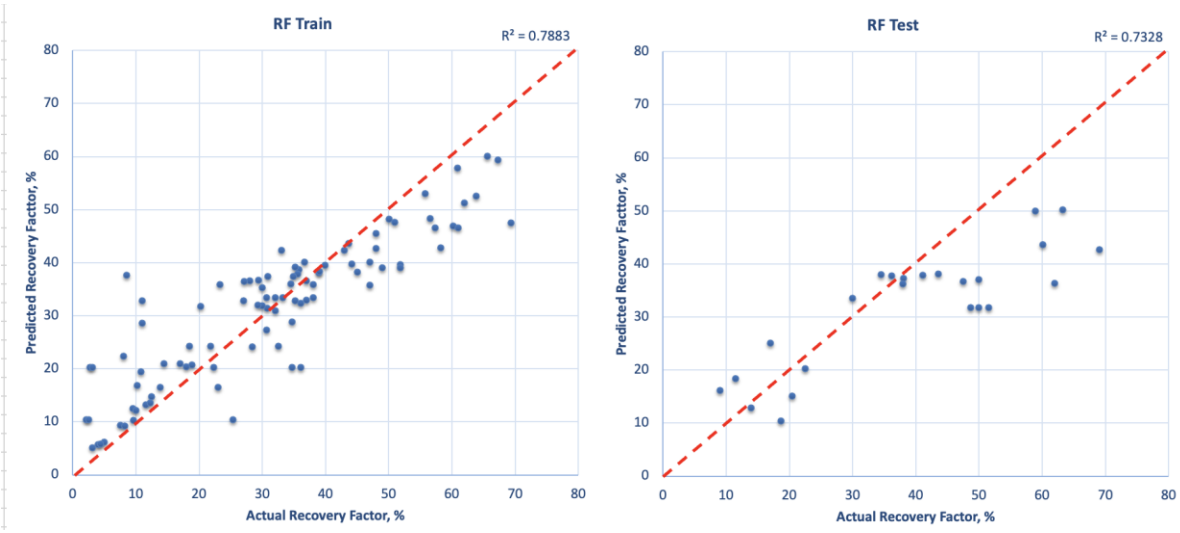

Figure 39. Results of R^2 for the RF Model for the Secondary Dataset

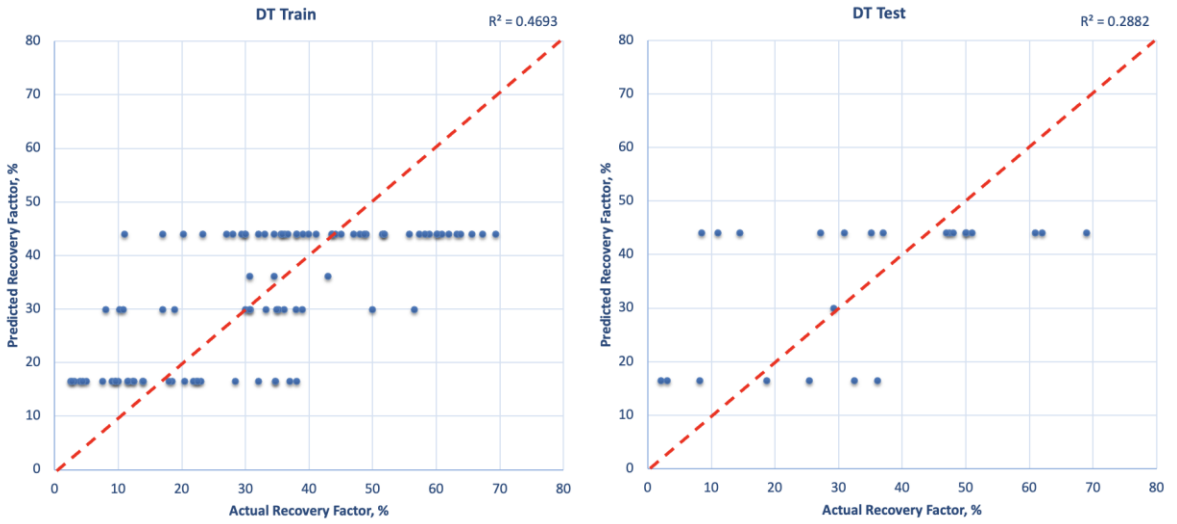

Figure 40. Results of R^2 for the DT Model for the Secondary Dataset

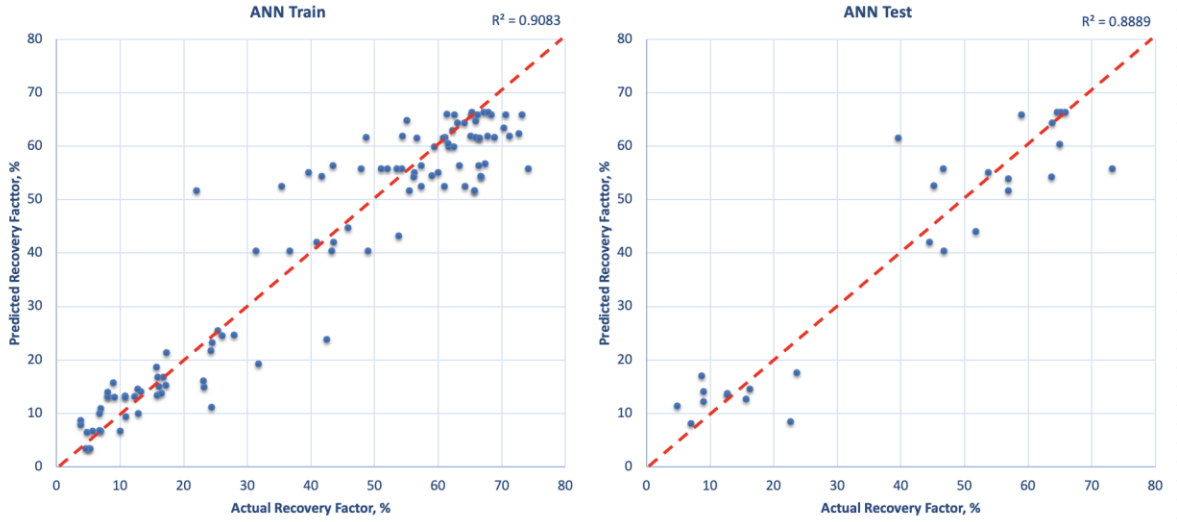

Figure 41. Results of R^2 for the ANN Model for the Tertiary Dataset

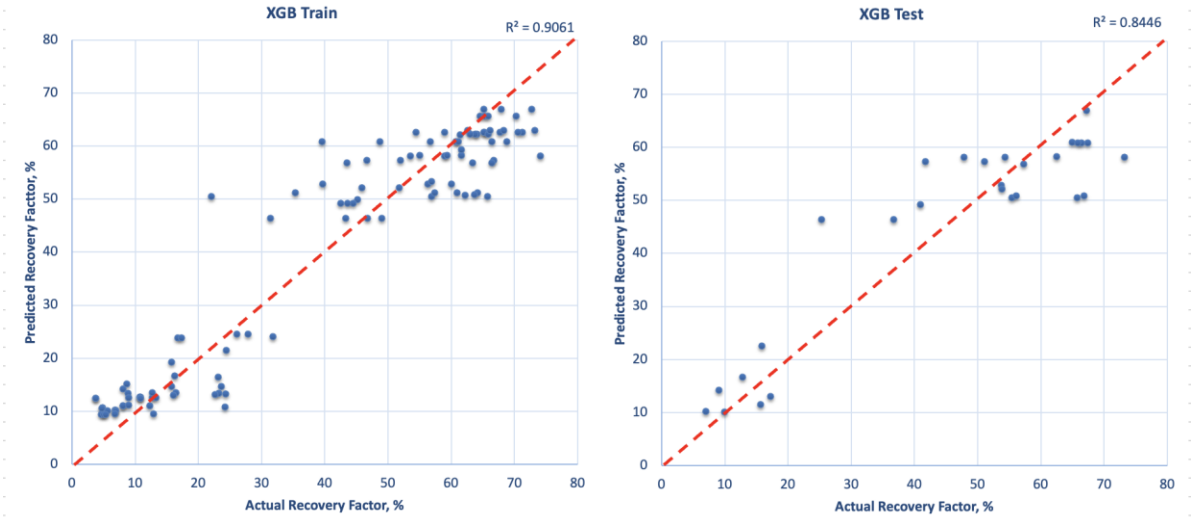

Figure 42. Results of R^2 for the XGB Model for the Tertiary Dataset

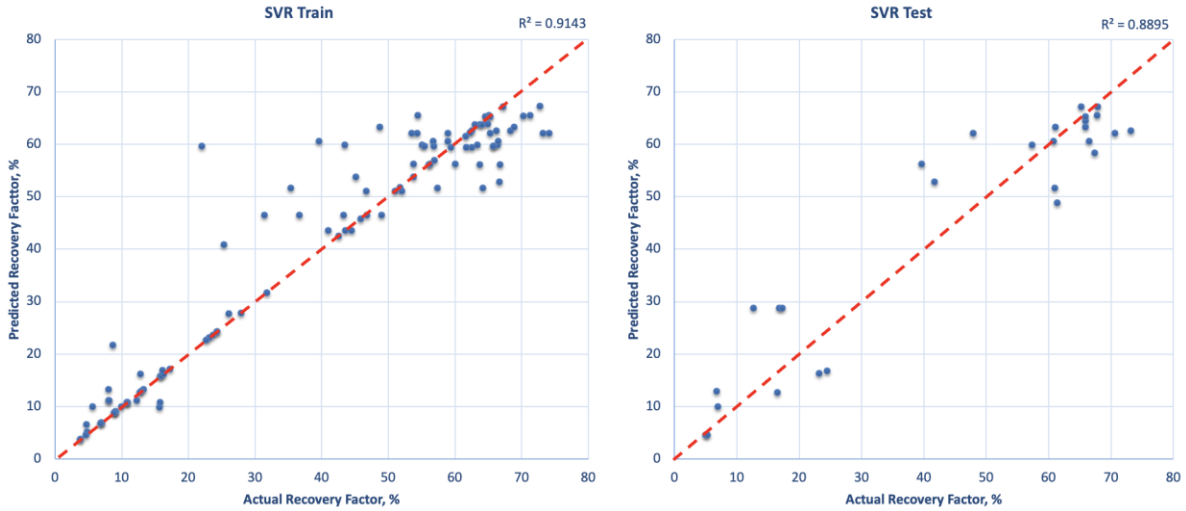

Figure 43. Results of R^2 for the SVR Model for the Tertiary Dataset

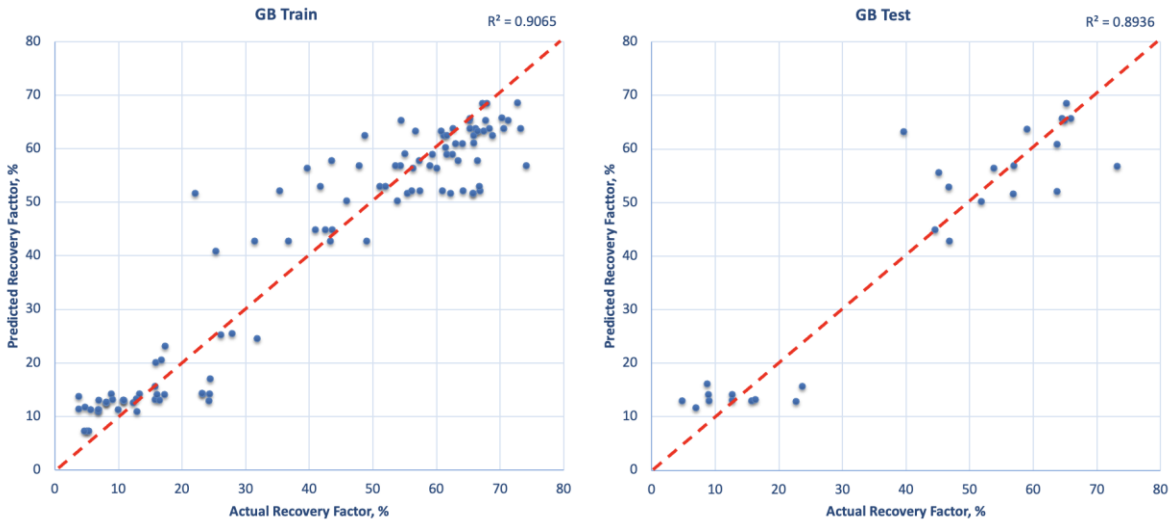

Figure 44. Results of R^2 for the GB Model for the Tertiary Dataset

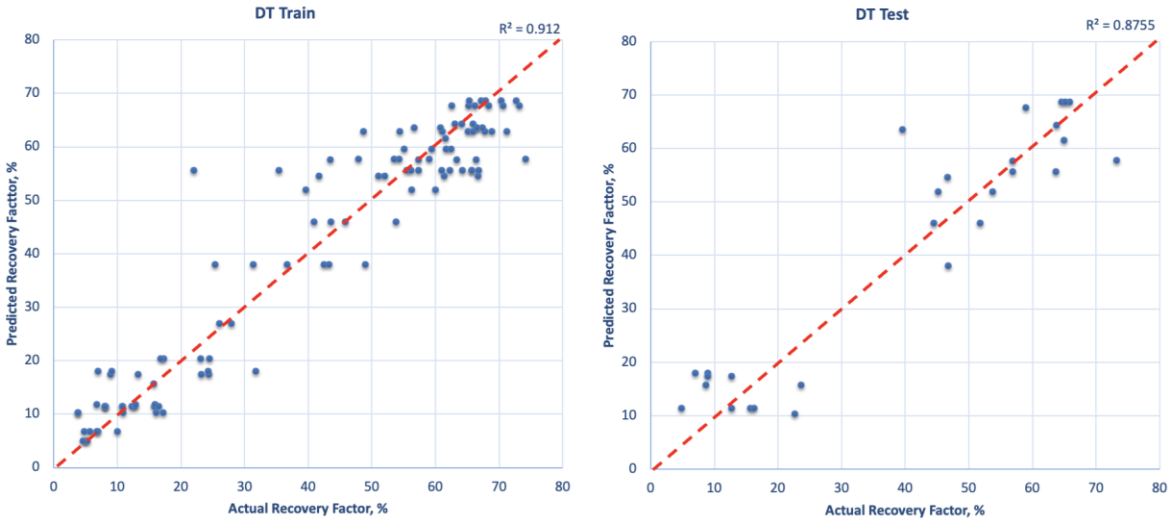

Figure 45. Results of R^2 for the DT Model for the Tertiary Dataset

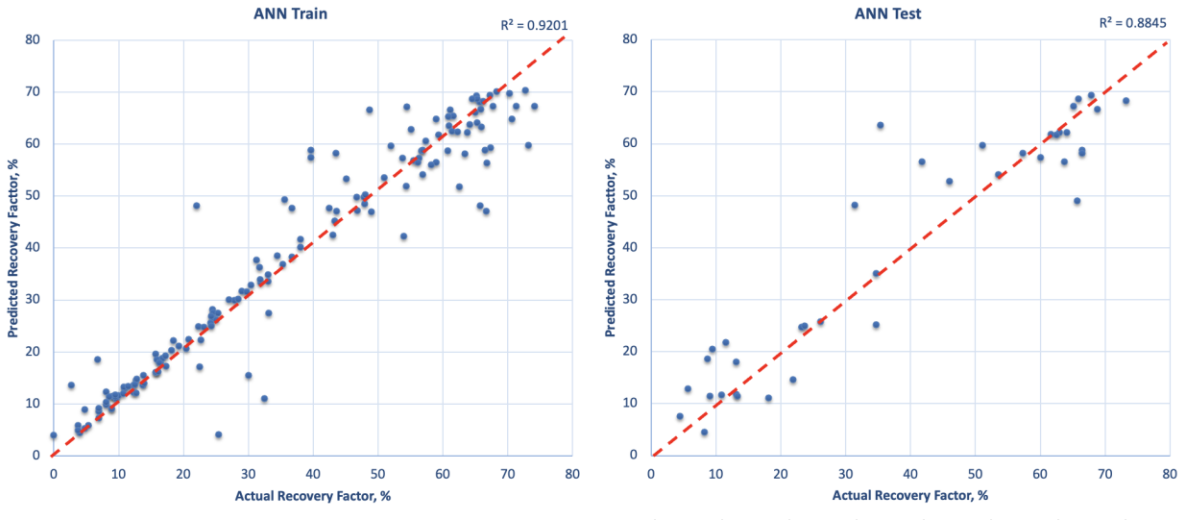

Figure 46. Results of R^2 for the ANN Model for Both Datasets

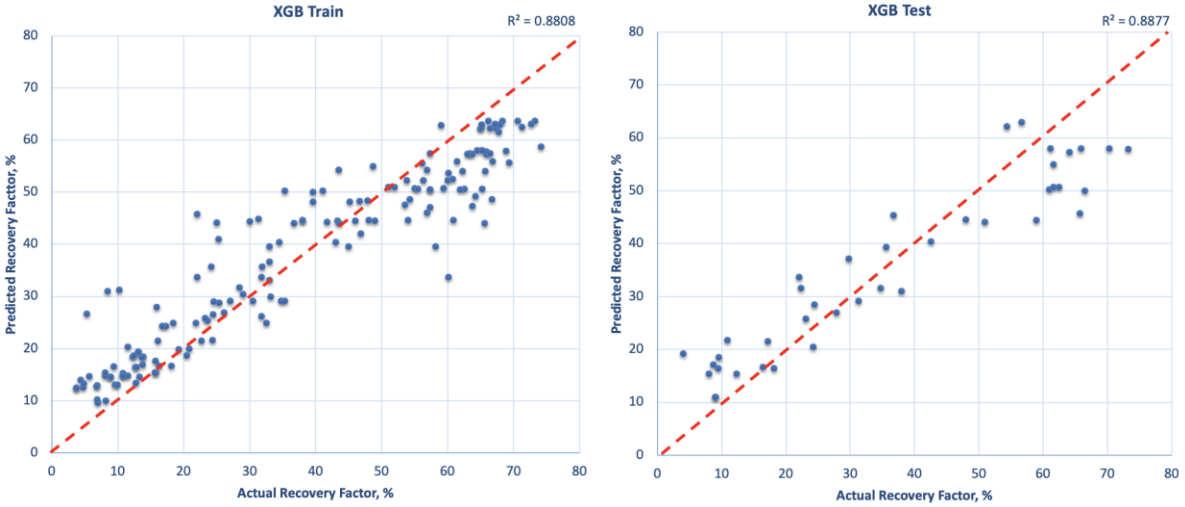

Figure 47. Results of R^2 for the XGB Model for Both Datasets

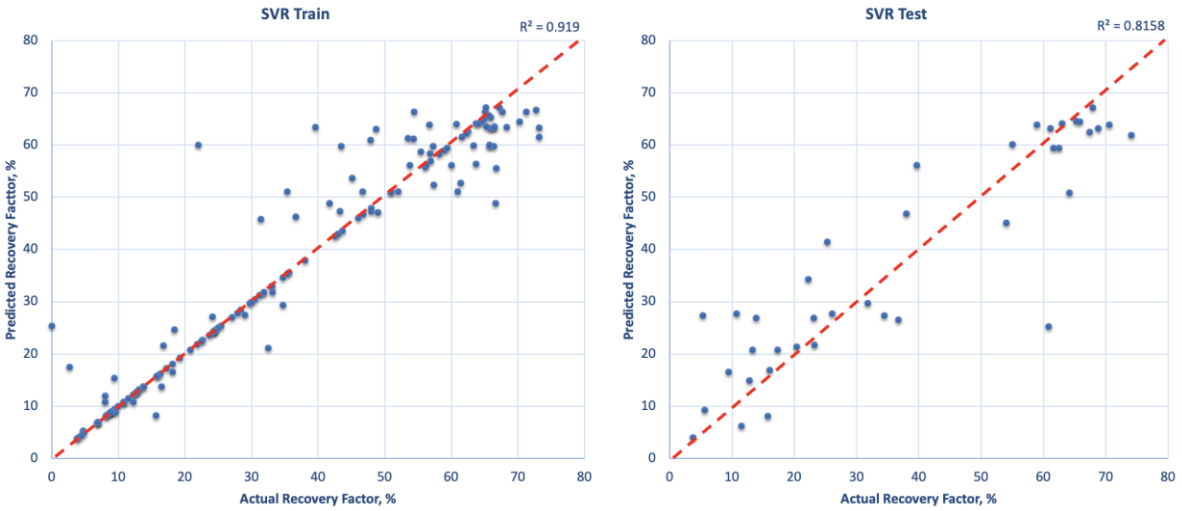

Figure 48. Results of R^2 for the SVR Model for Both Datasets

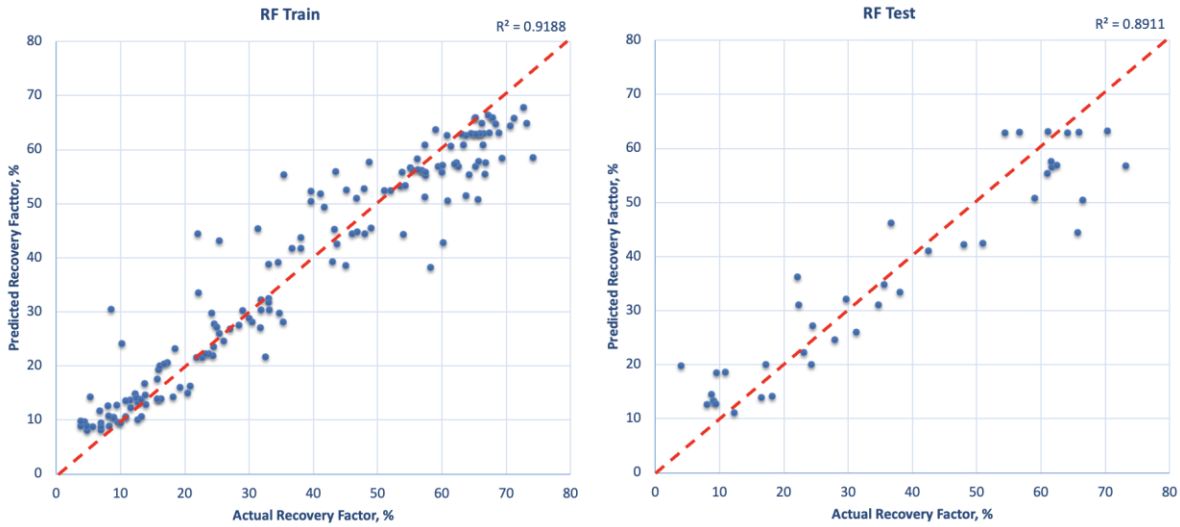

Figure 49. Results of R^2 for the RF Model for Both Datasets

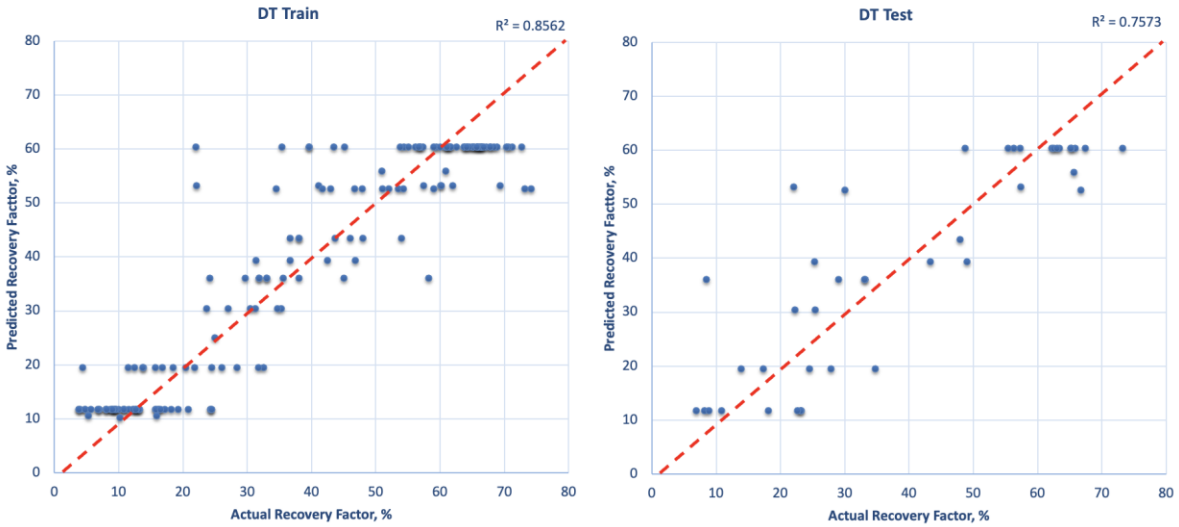

Figure 50. Results of R^2 for the DT Model for Both Datasets